Altered structural organization and functional connectivity in feedforward neural networks after induced perturbation

Janelle S. Weir[1]*, Katrine Sjaastad Hanssen[1,2]*, Nicolai Winter-Hjelm[1], Axel Sandvig[1,3], Ioanna Sandvig[1]

[1]Department of Neuromedicine and Movement Science, Faculty of Medicine and Health Sciences, Norwegian University of Science and Technology (NTNU), Trondheim, Norway
[2] Kavli Institute for Systems Neuroscience, NTNU, Trondheim, Norway
[3] Department of Neurology and Clinical Neurophysiology, St Olav´s University Hospital, Trondheim, Norway

***These authors share first co-authorship**
Correspondence: janelle.s.weir@ntnu.no, katrine.s.hanssen@ntnu.no , ioanna.sandvig@ntnu.no

Keywords: Cortical network; neural engineering; electrophysiology; mutated tau; self-organization; neuroplasticity

Abstract

Reciprocal structure–function relationships underly both healthy and pathological behaviors in complex neural networks. Neuropathology can have widespread implications on the structural properties of neural networks, and drive changes in the functional interactions among network components at the micro- and mesoscale level. Thus, understanding network dysfunction requires a thorough investigation of the complex interactions between structural and functional network reconfigurations in response to perturbation. However, such network reconfigurations at the micro- and mesoscale level are often difficult to study *in vivo*. For example, subtle, evolving changes in synaptic connectivity, transmission, and electrophysiological shift from healthy to pathological states are difficult to study in the brain. Engineered *in vitro* neural networks are powerful models that enable selective targeting, manipulation, and monitoring of dynamic neural network behavior at the micro- and mesoscale in physiological and pathological conditions. In this study, we first established feedforward cortical neural networks using in-house developed two-nodal microfluidic chips with controllable connectivity interfaced with microelectrode arrays (mMEAs). We subsequently induced perturbations to these networks by adeno-associated virus (AAV) mediated expression of human mutated tau in the presysnaptic node and monitored network structure and activity over three weeks. We found that induced perturbation in the presynaptic node resulted in altered structural organization and extensive axonal retraction starting in the perturbed node. Perturbed networks also exhibited functional changes in intranodal activity, which manifested as an overall decline in both firing rate and bursting activity, with a progressive increase in synchrony over time. We also observed impaired spontaneous and evoked internodal signal propagation between pre-and postsynaptic nodes in the perturbed networks. These results provide novel insights into dynamic structural and functional reconfigurations in engineered feedforward neural networks as a result of evolving pathology.

1. Introduction

An understanding of dynamic structure-function relationships in neural networks in health and disease remains a subject of intense investigation. Such dynamics involve micro- and mesoscale level interactions over different temporal scales. Mechanisms that drive the reciprocal relationship between network structure and function involve Hebbian and homeostatic plasticity working in tandem. These plasticity mechanisms influence pre- and postsynaptic connectivity Henderson and Gong (Henderson et al., 2018), excitatory – inhibitory synaptic transmission (Moore et al., 2018), and hierarchical processing between different areas of the network (Rubinov et al., 2009; Yamamoto et al., 2018). These mechanisms are also inextricably linked both physiologically and pathophysiologically. This means that perturbation within one part of the network can progressively spread and impact other parts through axonal and/or synaptic connections. Furthermore, network impairment may evolve over a long period of time without overt manifestation of dysfunction (Fornito et al., 2015). For example, in neurological diseases which significantly impact the structural and functional integrity of the network, such as Alzheimer's disease (AD), relevant network reconfigurations due to evolving pathology (Katsuno et al., 2018) tend to occur over a long period of time before the emergence of clinical symptoms, by which point, the network has undergone considerable, irreversible damage (reviewed in (Tarawneh et al., 2012).

One of the main structural pathological hallmarks of AD is the accumulation of neurofibrillary tangles in the brain as a result of the hyperphosphorylation of the microtubule associated protein tau (Braak et al., 1991). Tau proteins are mainly found in the axons of neurons and, under physiological conditions, (Götz et al., 2019) they enrich microtubules to promote their assembly in axons (Baas et al., 2019; Qiang et al., 2018). However, under pathological conditions, tau becomes hyperphosphorylated, causing widespread morphological disruption in axons (Jackson et al., 2017; Kopeikina et al., 2013), ultimately affecting synaptic transmission and network function. The high interconnectivity of the brain also implies that neuronal axons and synapses may act as conduits for the spread of such pathology from affected areas, causing progressive, widespread disruption to the structural and functional integrity of the network (Kuhl, 2019). It has also been shown that hyperphosphorylated tau triggers hypoactivity in neurons (Ittner et al., 2011; Menkes-Caspi et al., 2015; Polanco et al., 2018; Wang et al., 2017), thus disturbing excitatory-inhibitory balance, and disrupting synaptic transmission and global integration across the network.

To elucidate how relevant pathological mechanisms gradually affect the structure and function of neural networks, it is imperative to study the underlying processes at the micro- and mesoscale. Such investigations are highly challenging, or de facto not feasible *in vivo* due to the size and complexity of

the brain. This challenge can be overcome with the application of advanced cellular models based on engineered neural networks. Such networks develop with progressively increasing structural and functional complexity over time, essentially recapitulating fundamental aspects of neural network behavior as seen in the brain (Collingridge et al., 2010; Valderhaug et al., 2021; van de Wijdeven et al., 2019; Winter-Hjelm N, 2023). Engineered *in vitro* models thus enable longitudinal studies of dynamic network behavior and allow for selective perturbation and monitoring of network responses at the micro- and mesoscale level (Bauer et al., 2022; Bruno et al., 2020; Fiskum et al., 2021; Gribaudo et al., 2019; Nonaka et al., 2011; Valderhaug et al., 2021; Weir et al., 2023).

In the present study, we longitudinally investigated structural and functional changes in engineered two-nodal feedforward cortical neural networks, following induced expression of human mutated tau in the presynaptic nodes. Our primary aim was to longitudinally monitor and identify dynamic changes in neurite organization and electrophysiological activity of networks with evolving perturbation and compare this with control unperturbed networks. The two-nodal feedforward configuration of the engineered network enabled us to observe structural and functional reconfigurations in response to the perturbation in the affected node, while simultaneously monitoring dynamic changes in the postsynaptic node. Our results demonstrate that prior to perturbation, all neural networks developed increasingly robust firing and bursting activity within the nodes. They had also developed prominent structural connections, and functional internodal connections with spontaneous and evoked feedforward burst propagation from the presynaptic to postsynaptic nodes. However, within four days of inducing perturbation by expression of human mutated tau in the presynaptic node, internodal connectivity was disrupted, manifested as progressive retraction of neurites from the entry zone near microtunnels in the presynaptic node, followed by retraction of neurites from the exit zones near the microtunnels towards the postsynaptic nodes. Neurite retraction persisted over a span of 3 weeks, during which period we observed a concomitant significant reduction in the overall intranodal mean firing rate, mean burst rate, and total number of bursts. Such structural or functional changes were not observed in control unperturbed networks. Furthermore, the neurite retraction and overall decrease in activity in the perturbed networks occurred simultaneously with a significant increase in network synchrony. Increased synchrony over time was not observed in control unperturbed networks. These results provide new insights into dynamic micro- and mesoscale network reconfigurations in response to induced perturbations and illustrate the utility of engineered feedforward neural networks as models of network function and dysfunction.

102 # 2. Methods

103

104 ## 2.1. *In vitro* neural networks

105 An experimental timeline can be found in **Figure 1**. For this study, we used in-house developed
106 microfluidic chips interfaced with microelectrode arrays (mMEAs; n=7) and 8-well chambered slides
107 (Ibidi, 80841; n=2). Design and fabrication of the mMEAs was conducted as reported previously by our
108 group (Winter-Hjelm N, 2023). Briefly, two compartments (from here on referred to as nodes) (5 mm
109 wide/60 µm high) were connected by 20 microtunnels (700 µm long/10 µm wide/5 µm high) designed
110 to promote unidirectional axonal outgrowth from the presynaptic to the postsynaptic node. Tesla
111 valve microtopographies were included in the microchannels to redirect axons from the postsynaptic
112 node back to their chamber of origin. Furthermore, axon traps were included on the postsynaptic side
113 to misguide outgrowing axons and prevent them from entering the microtunnels. To prevent neuronal
114 somata from entering the microtunnels, 4 µm pillars with 4 µm interspacing were positioned within
115 the presynaptic node. This design promotes formation of feedforward networks by aiding axon
116 outgrowth from the presynaptic node, but not vice versa. Impedance measurements and sterilization
117 of the mMEAs were conducted as reported previously (Winter-Hjelm N, 2023). Prior to seeding, nodes
118 were coated with 0.1 mg/mL Poly-l-Ornithine (PLO; Sigma-Aldrich, #P4957) for 30 min, subsequently
119 replenished with fresh PLO for another 2h at 37°C/5% CO_2. Following this, all PLO was discarded, and
120 the surfaces rinsed three times with distilled Milli-Q-water. Subsequently, the platforms were coated
121 with laminin solution consisting of 16 µg/mL Mouse Natural Laminin (Gibco, #23017015) diluted in
122 PBS (Sigma-Aldrich, D8537) for first 30 min, before being replenished with fresh laminin solution for
123 another 2 h at 37°C/5% CO_2. To ensure proper flow of coating solution through the microtunnels, a
124 hydrostatic pressure gradient was applied during all coating steps. Laminin solution was discarded and
125 replaced by astrocyte media consisting of DMEM (Gibco™, 11885084) supplemented with 15% Fetal
126 Bovine Serum (Sigma-Aldrich, F9665) and 2% Penicillin-Streptomycin (Sigma-Aldrich, #P4333) for 10
127 min at 37°C/5% CO_2 before rat primary cortical astrocytes (Gibco, #N7745100) were plated at a density
128 of 100 cells/mm^2 48 hours prior to plating of neurons Subsequently, rat primary cortical neurons
129 (Gibco, #A1084001) were plated at a density of 1,000 cells/mm^2 in neuronal media consisting of
130 Neurobasal Plus Medium (Gibco™, A3582801) supplemented with 2% B27 Plus Medium (Gibco™,
131 A358201), 2.5 mL/L Gluta-Max (Gibco™, 35050038) and 1% Penicillin-Streptomycin (Sigma-Aldrich,
132 P4333). 4 and 24 hours after plating the neurons, 90% of the media was replenished. Thereafter, 50%
133 of the media was replenished every 2 days.

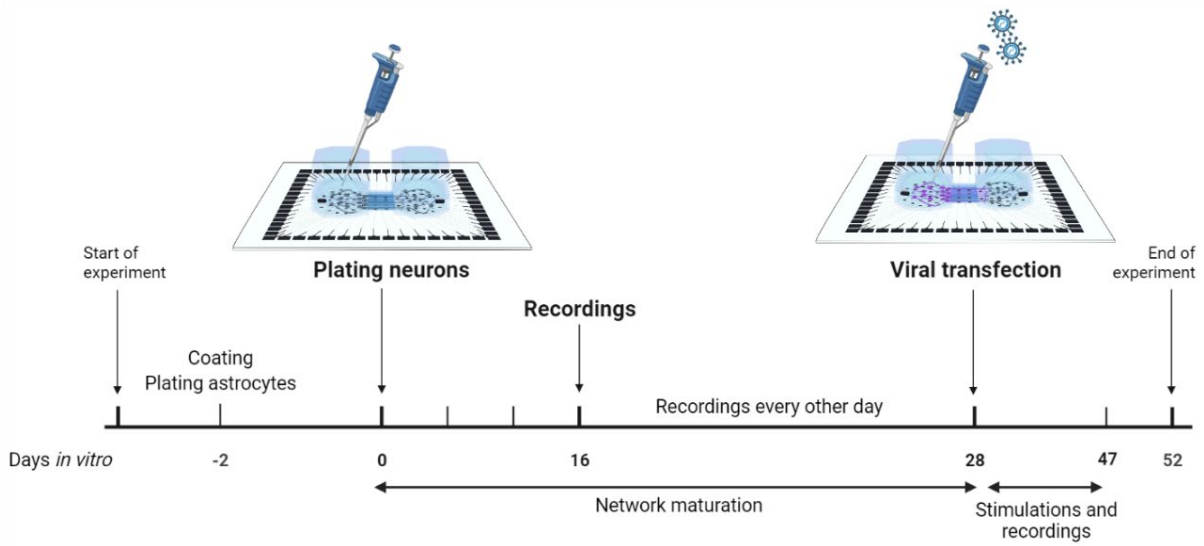

Figure 1. Schematic of the *in vitro* experimental timeline for establishing networks, transduction, and electrophysiological recordings. *Created with BioRender.com.*

2.1.1. AAV8 – GFP – 2A P301L Tau production and *in vitro* transduction

The viral vector was kindly gifted by Dr. Christiana Bjørkli (Department of Neuromedicine and Movement Science, NTNU). Adeno associated virus (AAV) vector production and purification was performed in-house at the Viral Vector Core Facility (Kavli Institute for Systems Neuroscience, NTNU). Tittering of the viral stock was determined as approximately 10^{11} vg/mL. Viral particles encoding experimental AAV8 P301L mutated tau were introduced to healthy networks at 28 DIV to induce perturbation. At 28 DIV, neurons were transduced by removing 70% of the cell media from the presynaptic nodes and directly adding 3 x 10^2 viral units per neuron diluted in cell media. After addition of the virus, the cultures were gently agitated for 30 s to ensure proper distribution of the viral particles and then incubated for 4 h. The titer of viral particles per neuron was decided after extensive tests of different concentrations. Afterwards, each well was topped up with fresh media without antibiotics and incubated for an additional 20 h at 37°C/5% CO_2. After the incubation period, 50% changes of the media were carried out as scheduled. To ensure comparable conditions with the control networks, an 80% media change was also conducted in the control unperturbed networks at the same time as the addition of AAV P301L to the perturbed networks. The viral vector encoded a GFP fluorescent tag for easy visualization of transduction efficiency.

2.2. Immunocytochemistry

To confirm network maturity including expression of phosphorylated tau (pTau) within the perturbed neural networks, immunocytochemistry (ICC) was performed at 22 DIV, as follows. Prior to immunostaining, cell media were aspirated and discarded from the culture plates, and the cultures were rinsed once with Dulbecco's Phosphate Buffered Saline (DPBS; Thermo Fischer Scientific, Cat

158 #14040-117). Following this, networks were fixed with 4% Paraformaldehyde (Sigma-Aldrich, #P6148)
159 for 10 min at room temperature followed by 3x10 min washes with DPBS. Further, all DPBS were
160 discarded and replaced by blocking solution consisting of 5% Goat serum (Sigma-Aldrich, Cat# G9023)
161 and 0.3% Triton-X (Thermo Fischer Scientific, Cat# 85111) in DPBS. Next, primary antibodies at the
162 indicated concentration (**Table 1**) were added in a buffer of 0.01% Triton-X and 1% Goat Serum in
163 DPBS overnight at 4°C. The following day, primary antibody solution was discarded, and cultures were
164 rinsed 3x5 min with DBPS before secondary antibodies at the indicated concentration (**Table 1**) were
165 added in a buffer of 0.01% Triton-X and 1% Goat Serum in DPBS for 2 h at room temperature. For
166 staining cellular nuclei, Hoechst dye (bisbenzimide H 33342 trihydrochloride; Sigma-Aldrich, Cat#
167 14533) was added at 1:10.000 dilution for the last 10 min of the secondary antibody incubation.
168 Samples from the 8-well Ibidi chips were washed with PBS, mounted on glass cover slides with anti-
169 fade fluorescence mounting medium (Abcam, Cat#Ab104135) whereas microfluidic chips were filled
170 with distilled Milli-Q-water before imaging.

171 **Table 1. List of primary and secondary antibodies with concentrations**

Primary antibodies	Concentration	Supplier
Ck Map2	1:1000	Abcam, #Ab5392
Rb Phospho-Tau (Thr217) (pTau)	1:1000	Invitrogen, #44-744
Ms AT8 (Ser202/205)	1:1000	Invitrogen, #MN1020
Rb GAD65/67	1:100	Abcam, #Ab183999
Ms Calmodulin (CaMKIIa)	1:200	Invitrogen, #MA3-918
Rb GFAP	1:500	Abcam, #Ab278054
Secondary antibodies	**Concentration**	**Supplier**
Goat-Anti-Mouse Alexa Fluor 674	1:1000	Invitrogen, #A21236
Goat-Anti-Rabbit Alexa Fluor 488	1:1000	Invitrogen, #A21244
Goat-Anti-Chicken Alexa Fluor 568	1:1000	Abcam, #Ab175477

172 *Ms: Mouse, Rb: rabbit, Ck: chicken.*

173

174 ### 2.2.1 Imaging

175 All samples from ICC were imaged using an EVOS M5000 microscope (Thermo Fischer Scientific,
176 #AMF5000) connected to a LED light source and using an Olympus 20x/0.75 NA objective (N1480500),
177 with the following filter sets/channels: DAPI (AMEP4650), CY5 (AMEP4656), GFP (AMEP4651) and
178 TxRed (AMEP4655). Phase contrast images were taken using a Zeiss Axio Vert V.1 brightfield 20x/53
179 WD/0.4 NA objective with an Axiocam 202 mono. Images were processed using Adobe Photoshop
180 2020. To quantify for fluorescent intensity profile of AT8 and pTau in cell body clusters and axonal
181 bundles in both perturbed and control unperturbed networks, fluorescent signal was measured in
182 Fiji/ImageJ2. A total of six clusters of cell bodies and five axonal bundles were selected as regions of
183 interest. Assessment was done for total fluorescent signal (mean intensity/pixel) measured by mean
184 grayscale.

185 **2.3. Electrophysiological recordings**

186 Electrophysiological activity of neural networks on mMEAs (n=7) was recorded using a MEA2100
187 recording system (Multichannel Systems, MCS, Reutlingen, Germany) at a sampling rate of 25,000 Hz.
188 A 3D-printed in-house made plastic cap covered by a gas-permeable membrane was used to keep the
189 cultures sterile during recordings. The stage temperature was set to 37°C (TC01, Multichannel
190 Systems) and the cultures were allowed to equalize on the stage for 5 min before spontaneous
191 electrophysiological activity was recorded for 15 min. All networks were recorded 24 h after media
192 changes on the following days *in vitro* (DIV): 16, 20, 24, 26, 28, 31, 33, 35, 37, 39, 41, 43, 45 and 47.
193 From 28 DIV onwards, networks were electrically stimulated and simultaneously recorded for 1
194 minute (directly following the 15 min recordings of spontaneous electrophysiological activity).
195 Electrical stimulations were applied to one presynaptic electrode with the highest detected mean
196 firing rate [21] during the 15 min recording. Stimulation consisted of a train of 60 spikes at ± 800 mV
197 (positive phase first) of 200 µs duration with an interspike interval of 5s. This was according to previous
198 studies demonstrating that persistent electrical stimulation in *in vitro* networks can increase network
199 activity over time, resulting in enhanced evoked action potentials and an increased frequency of spikes
200 in bursts (Brewer et al., 2009; Ide et al., 2010). Raw data was converted to an .h5 Hierarchical Data
201 Format using Multichannel DataManager (V.1.14.4.22018) system and imported to Matlab R2021b for
202 further analyses using adapted and custom-made scripts.

203

204 **2.4. Data analysis**

205 Electrophysiology data analysis was done as previously described (Winter-Hjelm N, 2023). Briefly, raw
206 data was filtered using a 4th order Butterworth bandpass filter removing low frequency fluctuations
207 below 300 Hz and high frequency noise above 3000 Hz. A notch filter was used to remove 50 Hz noise
208 caused by the power supply mains. Stimulation data was filtered using the SALPA filter (Wagenaar et
209 al., 2002), and each stimulation time point was followed by 15 ms blanking. Spike detection was
210 conducted using the Precise Timing Spike Detection (PTSD) algorithm (Maccione et al., 2009) with a
211 threshold of 11 times the standard deviation, a maximum peak duration set to 1 ms and a refractory
212 period of 1.6 ms. Burst detection was conducted using the logISI approach (Pasquale et al., 2010), with
213 a minimum of four consecutive spikes set as a minimum for a burst to be detected, and a hard
214 threshold of 100 ms. Network bursts were detected using the logIBEI approach (Pasquale et al., 2010),
215 with at least 20% of active electrodes required to participate during the span of a network burst.
216 Network synchrony was measured using the coherence index (Timme et al., 2018).

217 **2.5 Statistical analysis**

SPSS version 29.0.0.0 was utilized for all statistical analyses. For comparison of the repeated measures, we used Generalized Linear Mixed-Effect Models (GLMMs) with network type (i.e., controls versus perturbed networks) as a fixed effect, and the network characteristics as targets. The network age (DIV) was used as a random effect. Only data from 31 DIV onwards were included in the analysis to specifically compare changes in network characteristics following perturbation to the control unperturbed networks. A gamma probability distribution with a log link function was chosen as the linear model. This selection was based on the Akaike information criterion and initial assessment of distribution fit to the predicted values. For multiple comparisons, we used sequential Bonferroni adjustment.

227 # 3. Results

228 ## 3.1. Engineered feedforward cortical networks show intra- and internodal connectivity

229 Prior to perturbation, we wanted to validate that neurons were structurally connected with each other
230 within the nodes and expressed markers for excitatory and inhibitory synaptic transmission. Our
231 results showed that the engineered neural networks organized into densely interconnected intranodal
232 architectures, with outgrowing neurites in the microtunnels **(Figure 2A and B).** Additionally,
233 immunocytochemistry performed at 22 DIV revealed expression of the microtubule-associated
234 protein 2 marker, MAP2 **(Figure 2C and D)**, the inhibitory neuronal marker glutamic acid decarboxylase
235 65/67, (GAD65/67) (Fukuda et al., 1997) **(Figure 2C)**, and the excitatory neuronal marker calcium-
236 calmodulin (CaM) – dependent protein kinase II, (CaMKII) (Takao et al., 2005) **(Figure 2D)**. The
237 presence of these markers indicated that the networks consisted of mature neurons with the capacity
238 for excitatory and inhibitory synaptic transmission, a crucial aspect for achieving structural and
239 functional network maturity.

240 To investigate whether the engineered networks were functionally connected, we monitored and
241 recorded electrophysiological activity commencing at 16 DIV. By 26 DIV, the neural networks displayed
242 a mature electrophysiological profile in line with previous studies [19] (Chiappalone et al., 2006;
243 Winter-Hjelm N, 2023). Specifically, raster plots of spontaneous activity within the network revealed
244 both isolated spikes and synchronized bursts **(Figure 3A)**, while correlation matrices of network
245 connectivity showed strong connectivity within pre- and postsynaptic nodes, as well as functional
246 connectivity between the nodes **(Figure 3B)**. To further validate internodal connectivity, we applied
247 electrical stimulations to the electrode with the highest firing rate within the presynaptic node at 26
248 DIV. We recorded and assessed the evoked activity in the postsynaptic node, which revealed that
249 electrical stimulations caused a spiking response in the presynaptic node, followed by an on average
250 40 ms time delay before a subsequent spiking response was observed in the postsynaptic node **(Figure**
251 **3C)**. This effectively demonstrated that functional connectivity was established between the- pre and
252 postsynaptic nodes.

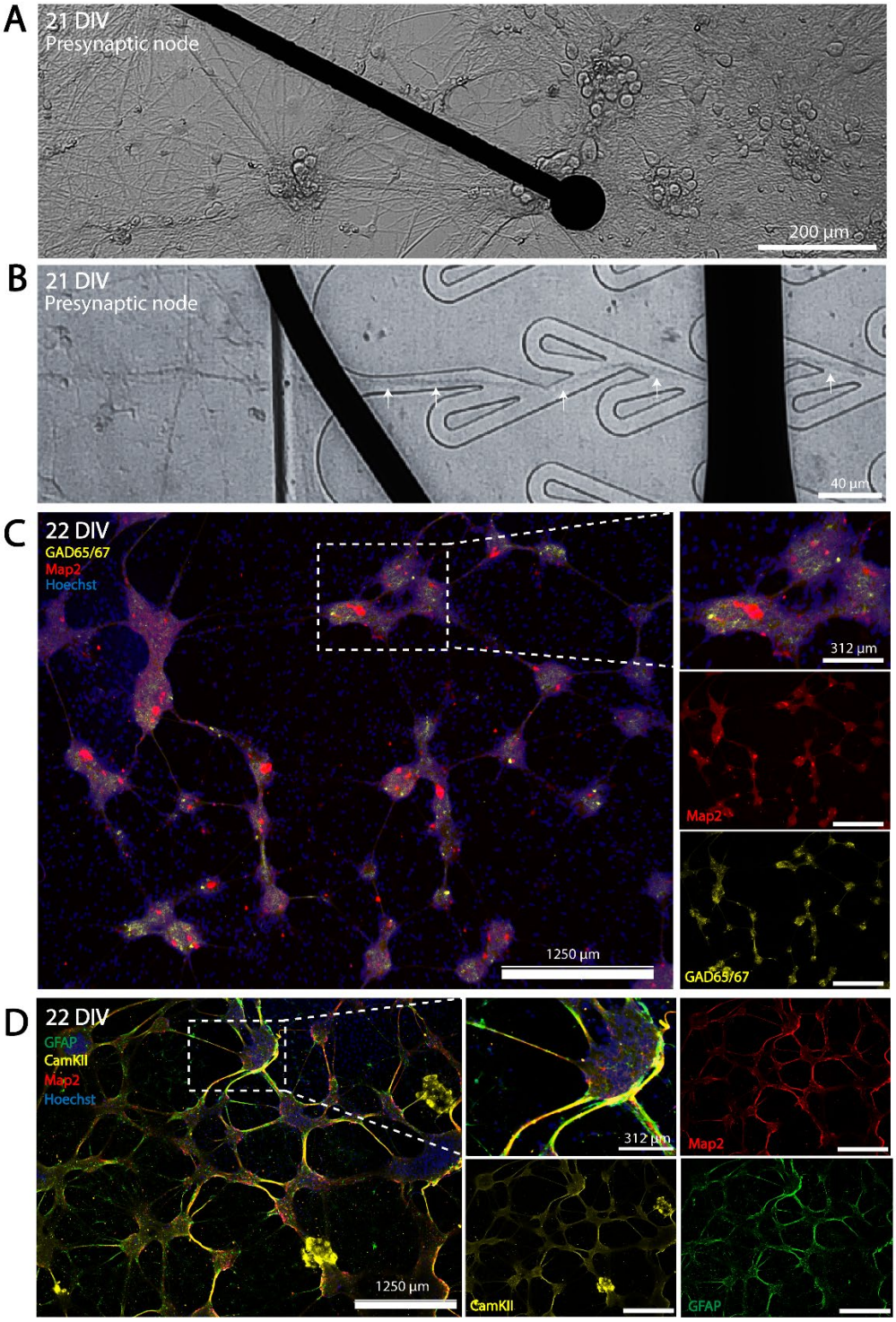

Figure 2. Developing structural organization and functional maturity of feedforward engineered neural networks (A-B) Phase contrast images of a neural network in the presynaptic node **(A)** with neurite projections going through the microtunnels **(B**) on a mMEA at 21 DIV. **(C-D)** Networks positively immunolabeled for the neuronal marker MAP2 in addition to the inhibitory marker GAD65/67 **(C)** and the excitatory neuron marker CaMKII **(D).** Glial fibrillary acidic protein (GFAP) antibody labelling of astrocytes in the network. DIV; days in vitro. Scale bar 1250 µm; (magnified area 312 µm).

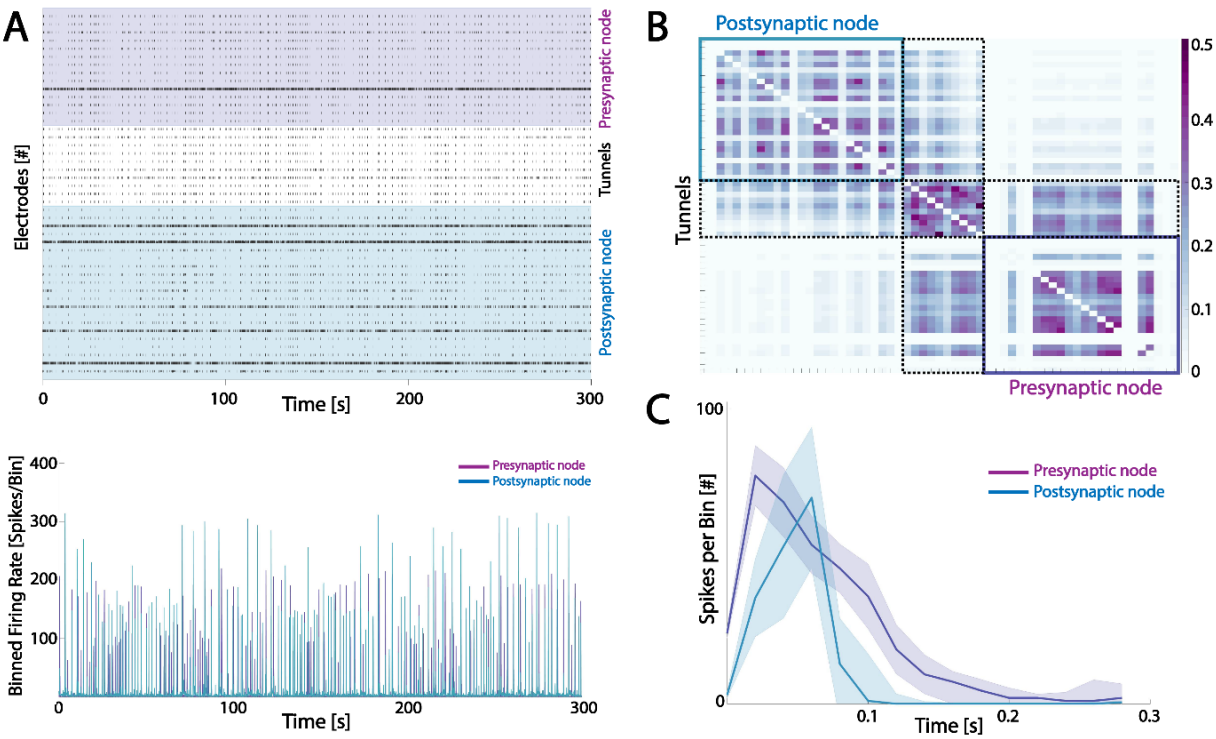

Figure 3. Neural networks displayed intra- and internodal functional connectivity at 26 DIV (A) Raster plots (300 seconds) of the recorded activity (top panel) and binned network activity (bottom panel) of corresponding total firing rate of one representative network. **(B)** Mutual information connectivity matrix showing the correlation in the network activity in nodes and tunnels. **(C)** Peristimulus time histogram of the pre- and postsynaptic response to an electrical stimulation in the presynaptic node. The graphs here show an initial response in the presynaptic node, followed by a delayed response in the postsynaptic node.

3.2. Perturbed networks express human mutated tau

At 28 DIV, we induced expression of human mutated tau protein in the presynaptic nodes of the engineered networks. The AAV construct encodes GFP, which allowed for easy visualization of transduction efficacy. Positive GFP expression was seen in the perturbed networks **(Figure 4B and Figure 5B)** which indicated effective AAV transduction. For additional verification of phosphorylated tau expression, we also labeled the networks for AT8 (Serine 202 and Threonine 205/ tau$^{202/205}$) and Phospho-Tau (Threonine 217/tau^{217}) proteins, hereon referred to as tau$^{202/205}$ and tau^{217}, respectively. Both tau$^{202/205}$ **(Figure 4B)** and tau^{217} **(Figure 5B)** were overexpressed in neuronal cytosols and axons along with GFP in perturbed networks. Healthy networks had higher fluorescent signal for tau$^{202/205}$ (Vale et al., 2010) in axonal bundles than perturbed networks, but lower fluorescent signal for tau^{217} in axonal bundles **(Figure 6)**. However, perturbed networks had significantly higher expression of both tau$^{202/205}$ and tau^{217} (Rajbanshi et al., 2023) in the cytosolic compartments compared to controls, while high expression of tau$^{202/205}$ was found in axon bundles. Additionally, we conducted primary exclusion immunolabeling for both tau$^{202/205}$ and tau^{217} to assess the specificity of the binding antigen, and no

expression was found **(Figure 4C and 5C respectively)**. We also performed secondary antibody exclusion to assess the labeling specificity of the primary antibody and found no immunoexpression for either tau$^{202/205}$ or tau^{217} in the networks.

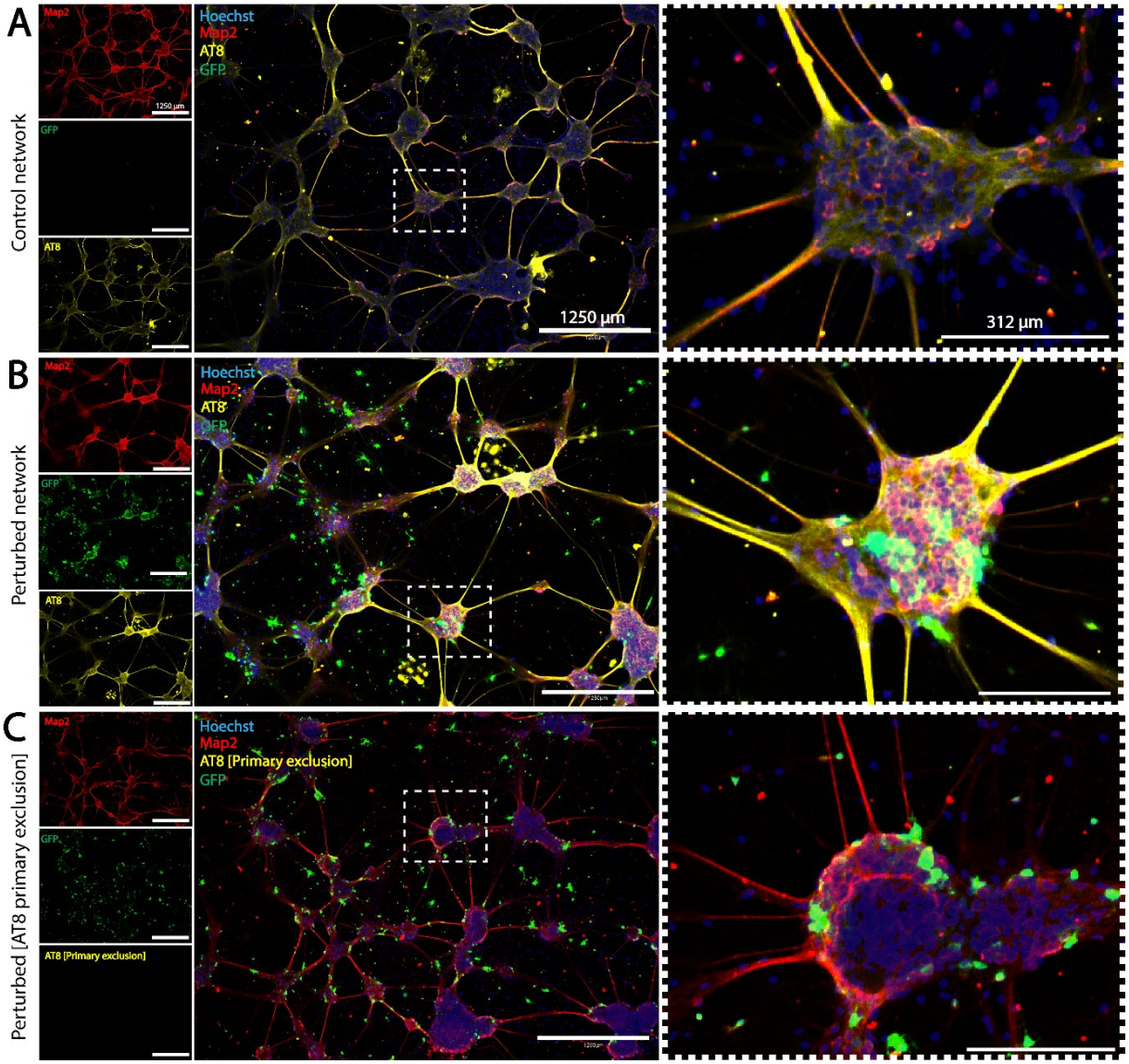

Figure 4. GFP expression exclusively in perturbed networks confirmed efficacy of viral transduction, further validated by AT8 expression. (A) Control unperturbed networks were not transduced with the AAV8-GFP-2A-P301L construct and thus did not express GFP. AT8 labeling was found primarily in axons. **(B)** Perturbed networks were positive for the GFP marker after transduction, with strong axonal and somato-dendritic AT8 expression. **(C)** Exclusion of the primary antibody AT8 to assess the specificity of antigen binding. Scale bar 1250 µm; (magnified area 312 µm).

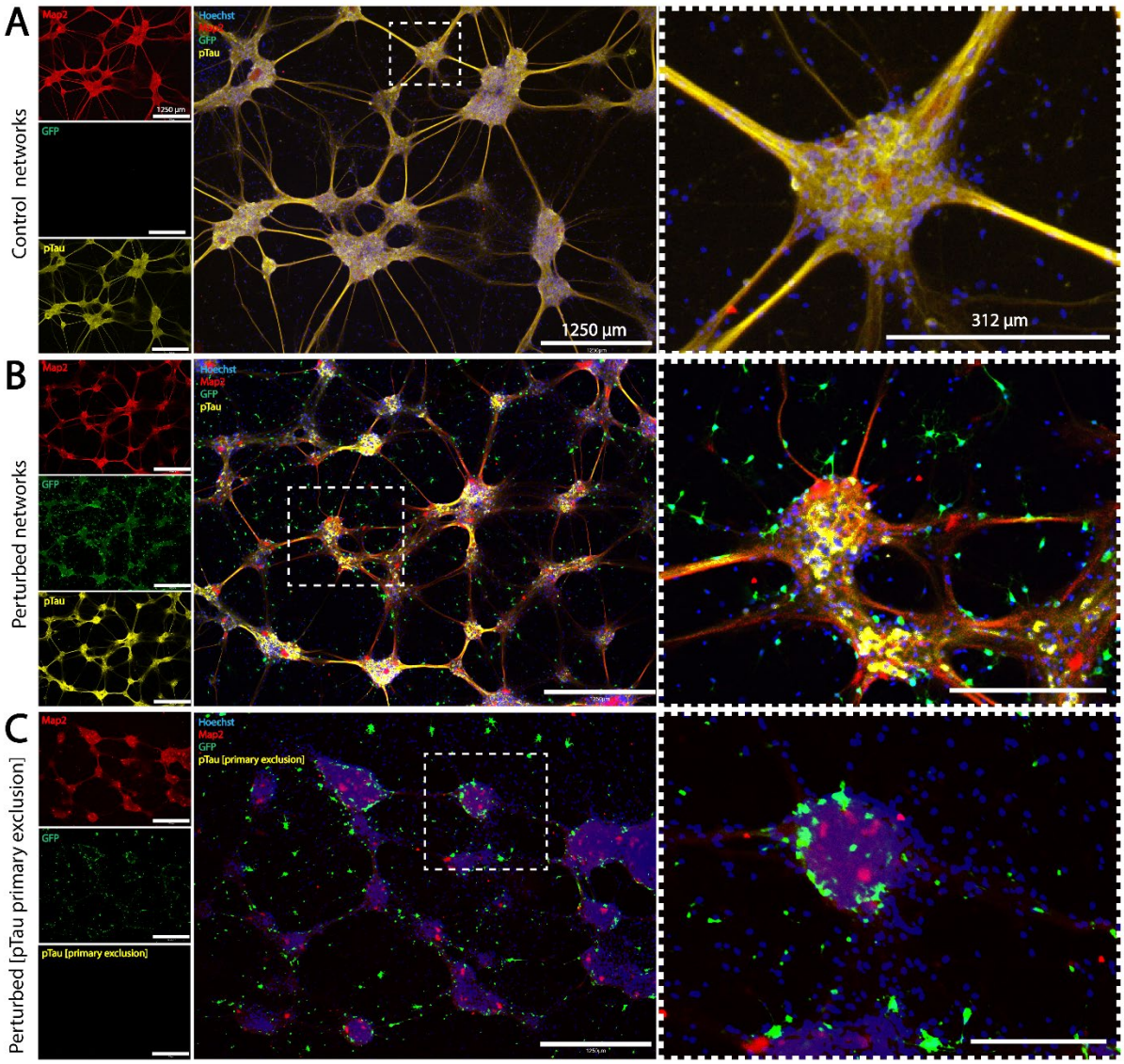

Figure 5. GFP expression exclusively in perturbed networks confirmed efficacy of viral transduction, further validated by pTau expression (A) Control unperturbed networks were not transduced with the AAV8-GFP-2A-P301L construct and thus did not express GFP. pTau labeling found in axons and cytosols. **(B)** Perturbed networks were positive for the GFP marker after transduction, with strong axonal and somato-dendritic pTau expression. **(C)** Primary exclusion of pTau to assess the specificity of antigen binding. Scale bar 1250 µm; (magnified area 312 µm).

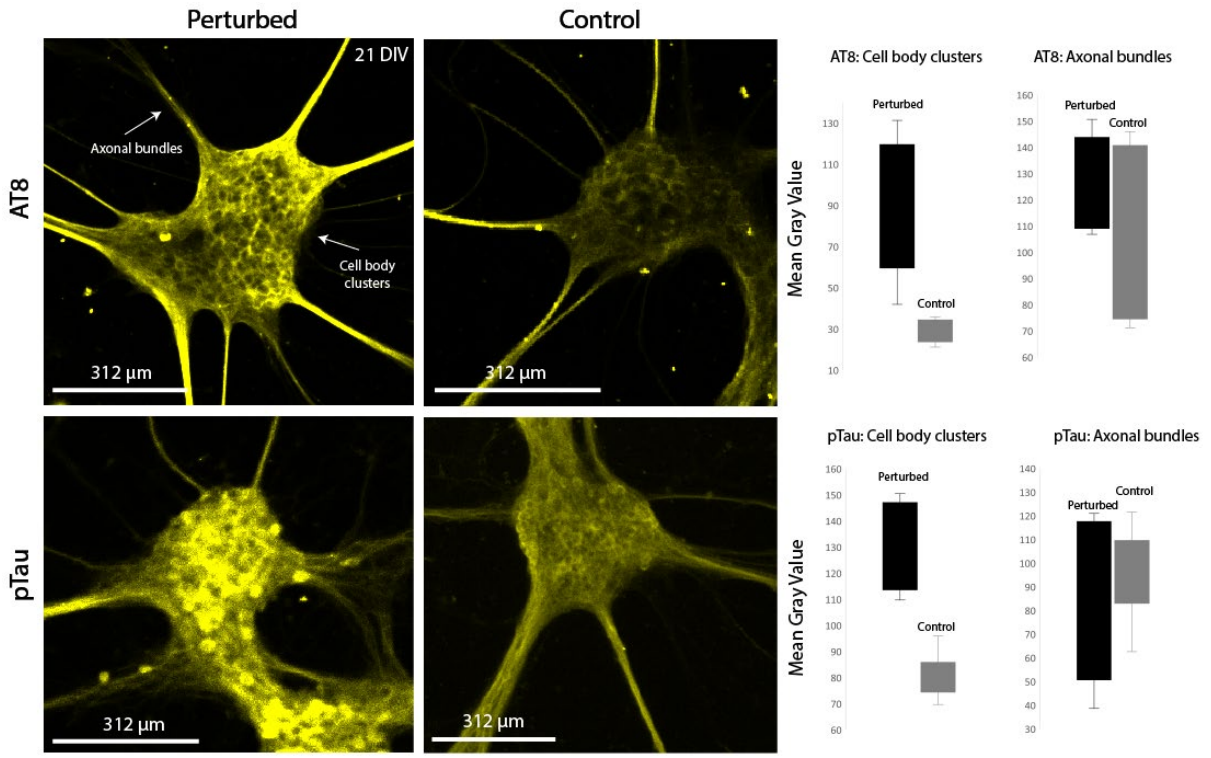

Figure 6. Quantification of fluorescent intensity of AT8 (tau$^{202/205}$) and pTau (tau^{217}) in perturbed and control networks. Representative images from networks with AT8 and pTau labelling showing cell body clusters and axonal bundles. Bar graphs showing the mean gray value of cell body clusters.

3.3. Progressive internodal axonal retraction observed after perturbation

Prior to induced perturbation, phase contrast imaging of neural networks at 21 DIV confirmed structural connections between the pre- and postsynaptic neural nodes **(Figure 7A).** Interestingly, by four days post perturbation, i.e., at 32 DIV, the neurites within the presynaptic node of the perturbed networks had started retracting from the entry zone near the unidirectional microtunnels, and by 52 DIV all structural connections between the presynaptic and postsynaptic nodes had been lost entirely **(Figure 7A).** Extensive neurite retraction was also observed in the postsynaptic node of the perturbed network by 52 DIV. In contrast, control unperturbed networks maintained robust neurite connections both at the entry zone of the presynaptic node microtunnels and the exit zone in the postsynaptic node **(Figure 7B).**

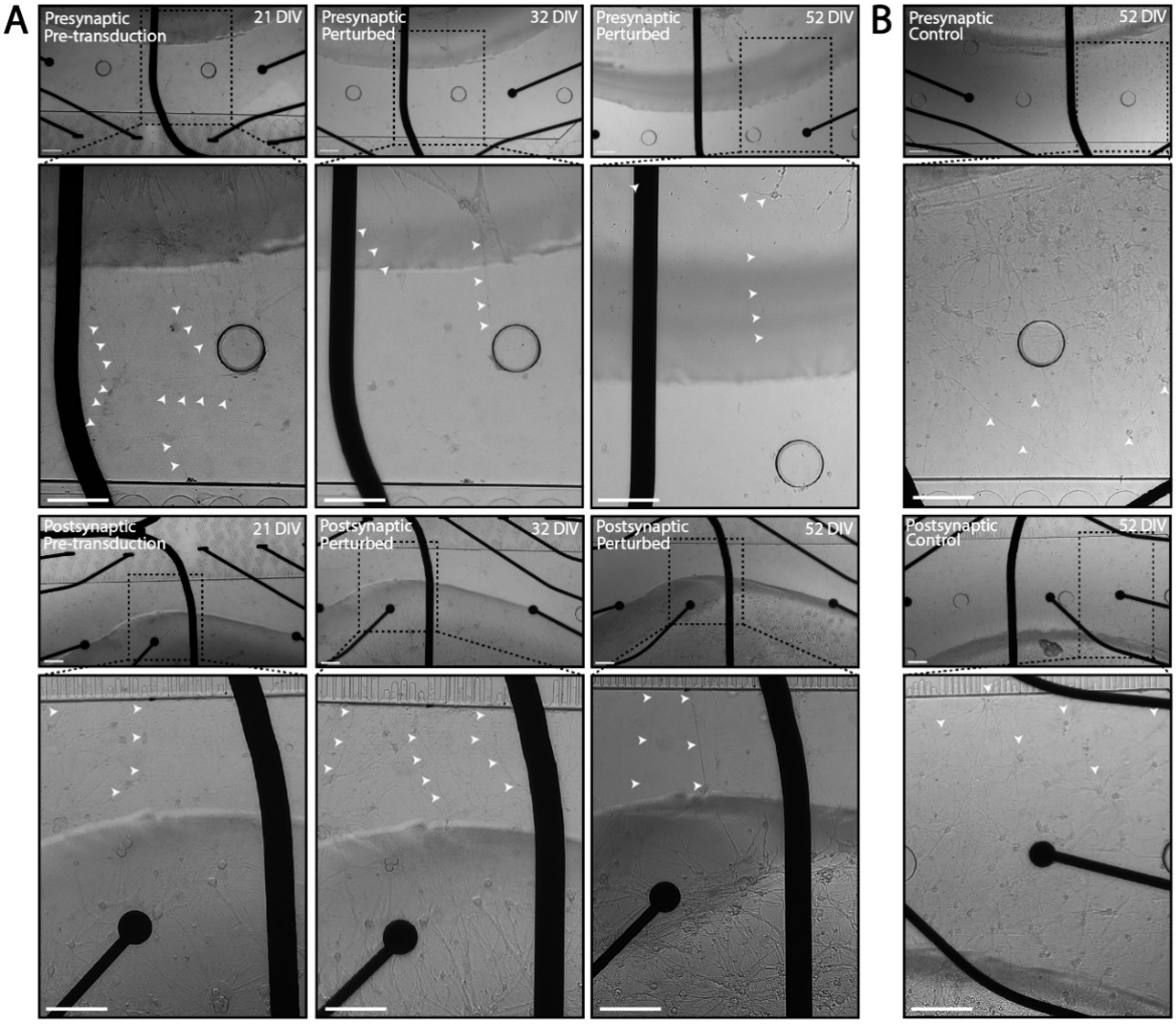

Figure 7. Progressive neurite retraction and active reorganization observed within networks following induced perturbation. (A) The leftmost column shows neurite extensions in the presynaptic node at the entry zone of the unidirectional microtunnels (top) and dense neurites in the postsynaptic node at the exit zone of the unidirectional microtunnels (bottom) at 21 DIV. The middle column is a snapshot of the same region in the network at 32 DIV showing retraction in the presynaptic node (top), but not in the postsynaptic node (bottom). The rightmost column shows extensive retraction in the presynaptic node (top) as well as in the postsynaptic node at 52 DIV (bottom). **(B)** Presynaptic (top) and postsynaptic (bottom) nodes of control unperturbed network depicting dense neurite connections at 52 DIV. Scale bar 100 µm.

3.4. Perturbed networks exhibit a decrease in overall network activity and an increase in network synchrony

Spontaneous network activity was recorded between 16 DIV and 47 DIV for both control unperturbed and perturbed networks. We captured network development from low activity to more mature profiles exhibited as increased mean firing rate **(Figure 8A)** and increased mean burst rate **(Figure 8B)**. Activity recorded from both pre- and postsynaptic nodes revealed the differences between healthy and perturbed networks and their functional evolution. Specifically, the presynaptic nodes of control unperturbed networks exhibited a steady increase in electrical activity between 16 DIV and 31 DIV, consistent with previous studies by us and others capturing developing functional activity in cortical networks (Wagenaar et al., 2006; Weir et al., 2023). Both firing rate and burst rate increased between 33 DIV and 45 DIV in the presynaptic node but not in the postsynaptic node **(Figure 8A and B, respectively)**.

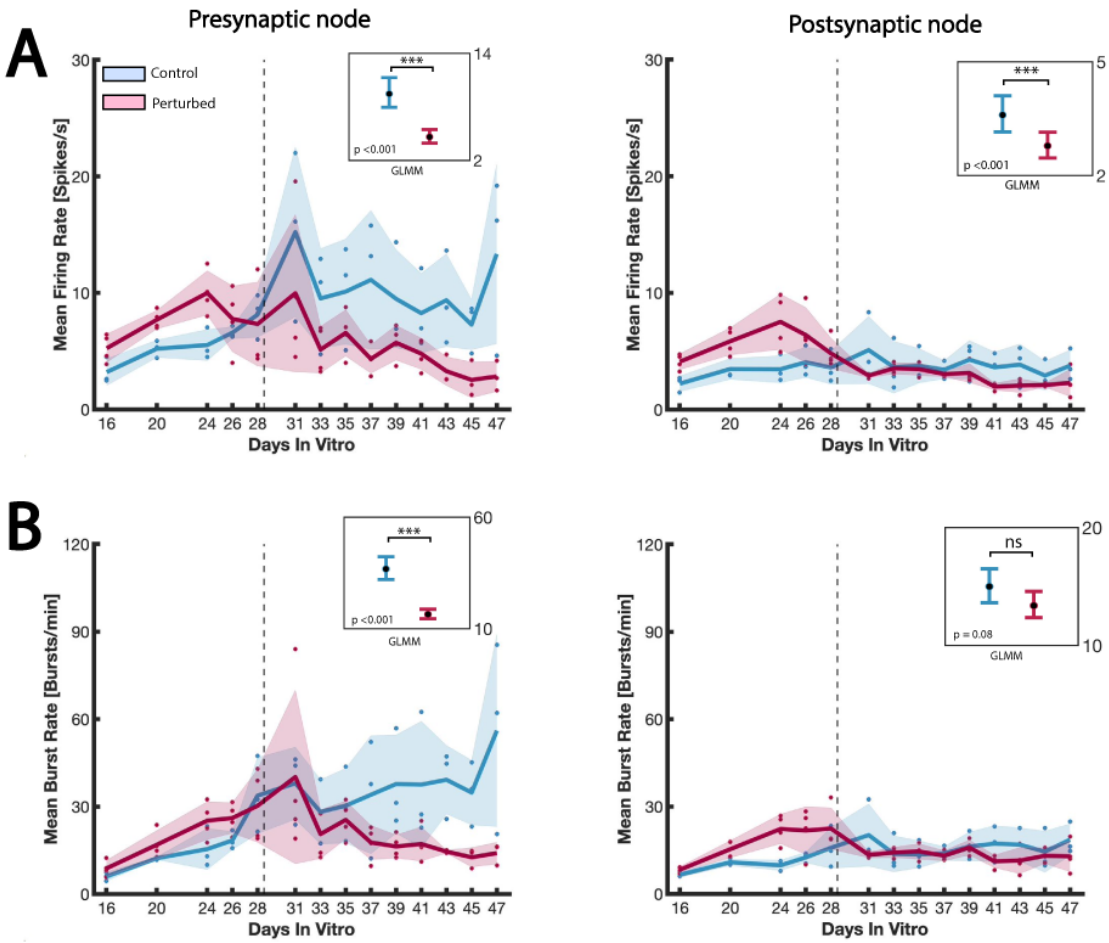

Figure 8. Electrophysiological recordings revealed progressive decrease in firing and burst rate in perturbed networks. (A) Mean firing rate (spikes/second) and **(B)** Mean burst rate (bursts/minute) in the presynaptic and post synaptic nodes for control unperturbed and perturbed networks. The solid lines denote the mean activity for the networks with the solid circles indicating individual data points. The shaded area denotes the standard error of the mean. The stippled line indicates the day of viral transduction in the perturbed networks (28 DIV).

342 Plots showing the GLMM estimated group averages with 95% confidence intervals are depicted in the top right
343 corner of the graphs.

344 Similarly, prior to induced expression of human mutated tau, the perturbed networks also exhibited
345 a steady increase in both firing rate and burst rate in the presynaptic node between 16 DIV and 28
346 DIV. However, between 31 DIV and 47 DIV, they exhibited significantly lower firing ($p< 0.001$) and
347 burst ($p< 0.001$) rates compared to healthy controls **(Figure 8A)**. The firing rate in the postsynaptic
348 node of perturbed networks remained significantly lower ($p< 0.001$) than controls for the duration of
349 the study **(Figure 8A)**. There were no significant differences in mean burst rate in the postsynaptic
350 node between healthy controls and perturbed networks **(Figure 8B).**

351 The postsynaptic node of healthy controls had significantly longer bursts ($p= 0.001$) compared to
352 perturbed networks **(Figure 9B)**, however, there were no significant differences in the mean burst
353 duration in the presynaptic nodes between perturbed and healthy controls between 31 DIV and 47
354 DIV **(Figure 9A).** Furthermore, the total network activity (pre- and postsynaptic node activity
355 combined) revealed that between 28 DIV and 47 DIV, healthy controls had significantly higher mean
356 network burst duration ($p< 0.001$) compared to perturbed networks **(Figure 9C)**. Specifically, between
357 28 DIV and 33 DIV, control unperturbed networks exhibited a transient increase in mean network
358 burst duration from 0.23 seconds to 0.26 seconds, however, there was a subsequent decrease
359 between 33 DIV and 47 DIV **(Figure 9C)**. For the perturbed networks, the total network activity for pre-
360 and postsynaptic nodes combined showed that between 33 DIV and 39 DIV there was a transient
361 increase in network burst duration from 0.17 seconds to 0.22 seconds, with a subsequent decrease
362 between 39 DIV and 47 DIV, similar to the healthy controls.

363 We also found that all networks had a general decrease in mean network burst size (analyzed as the
364 percentage of active electrodes participating in network bursts), between 16 DIV and 28 DIV **(Figure**
365 **9D)**. The total bursting activity for pre-and postsynaptic nodes combined showed that control
366 unperturbed networks decreased in burst size from 85% to 45% network participation **(Figure 9D)**
367 between 16 DIV and 28 DIV**.** Similarly, networks before perturbation had a decrease in burst size from
368 82% to 43% network participation **(Figure 9D)**. Both groups had relatively stable burst size between
369 28 DIV and 47 DIV, however, perturbed networks had significantly larger network bursts ($p< 0.001$) by
370 47 DIV (61% of network participation) compared to control unperturbed networks (45% network
371 participation) **(Figure 9D)**. Furthermore, when we examined network synchrony, measured by the
372 coherence index, we observed a general decrease in both pre-and postsynaptic nodes of healthy
373 controls between 16 DIV and 47 DIV **(Figure 9F)**. Both nodes of perturbed networks had progressively
374 increased synchrony that was significantly higher ($p< 0.001$) than in control unperturbed networks
375 between 31 DIV and 47 DIV **(Figure 9F)**.

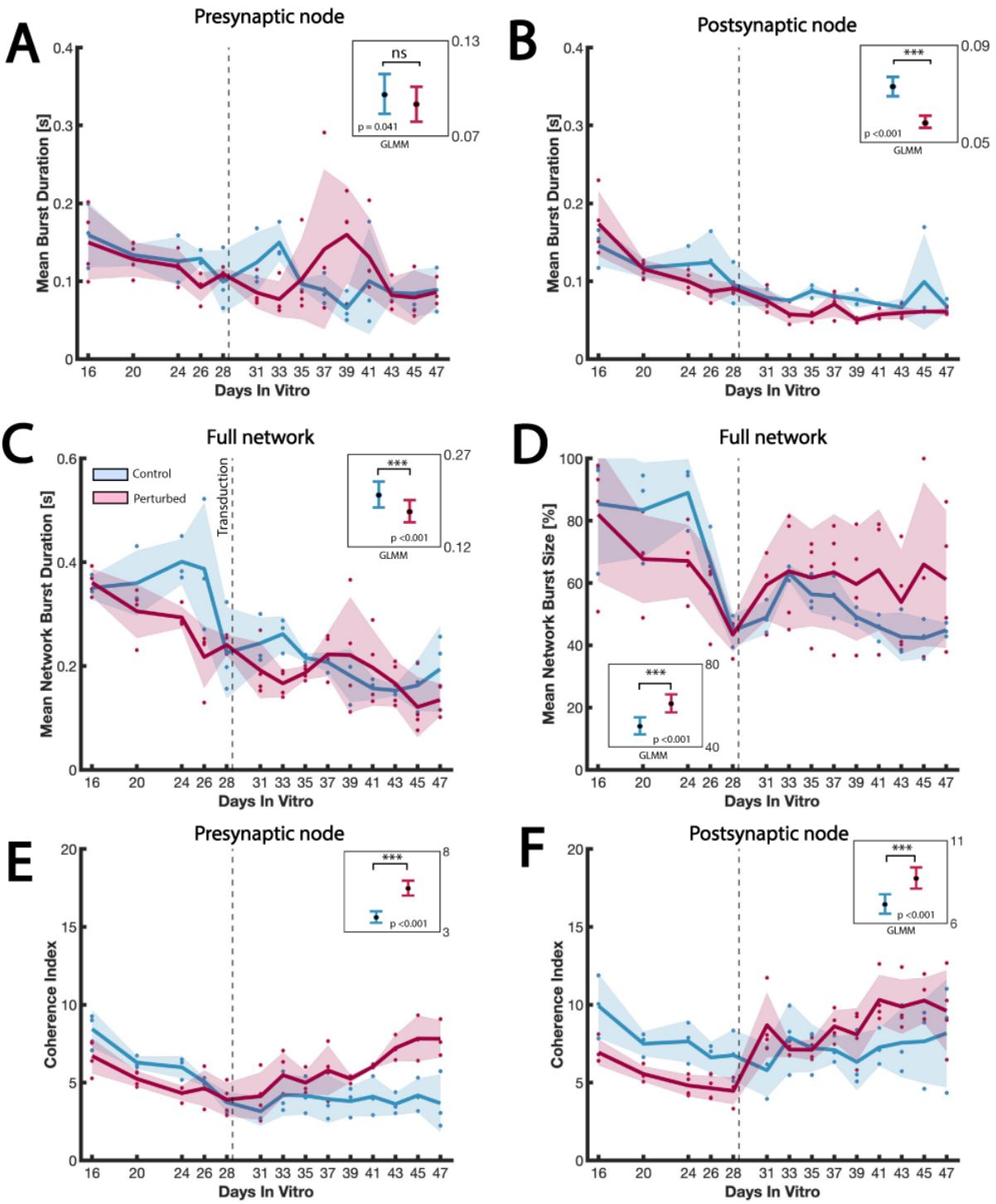

Figure 9. Electrophysiological recordings revealed a progressive increase in network burst size and synchrony in perturbed networks. (A) *Mean burst duration (seconds) in the pre-and* ***(B)*** *postsynaptic nodes of control and perturbed networks.* ***(C)*** *Mean network burst duration in the pre-and postsynaptic nodes combined for control and perturbed networks.* ***(D)*** *Mean network burst size (percentage) in the pre-and postsynaptic nodes combined for control and perturbed networks.* ***(E)*** *Coherence Index (measure of network synchrony) in the pre- and* ***(F)*** *postsynaptic nodes of control and perturbed networks. The solid line denotes the mean activity for the networks with solid circles indicating individual data points. The shaded area denotes the standard error of the mean. The stippled line indicates the day of transduction for the perturbed networks (28 DIV). Plots showing the GLMM estimated group averages with 95% confidence intervals are depicted in the top right corner of the graphs.*

3.5. Induced perturbation results in reduced propagation of spontaneous and evoked activity between nodes

Further analyses were conducted to determine the proportion of bursts propagating between the pre- and postsynaptic nodes in both control unperturbed and perturbed networks. We first evaluated the total number of network bursts exhibited by each network at each recording and identified the percentage of propagating bursts between the pre- and postsynaptic nodes in either direction **(Figure 10).** Our results showed that between 16 DIV and 28 DIV, both control unperturbed and perturbed networks had a steady increase in the total number of network bursts, with most or all bursts propagating in a feedforward manner from the presynaptic to the postsynaptic node **(Figure 10)**. Additionally, we found that for all subsequent recordings from 28 DIV onwards, burst propagation diminished in the control unperturbed networks to <2% by 47 DIV even though the total number of bursts within the network exceeded 2000 bursts/recording **(Figure 10)**. This implied that bursts were contained primarily within nodes of healthy controls. In contrast, perturbed networks exhibited a steady decline in the total number of network bursts between 33 DIV and 47 DIV (to less than10 bursts/recording by 43 DIV) **(Figure 10).**

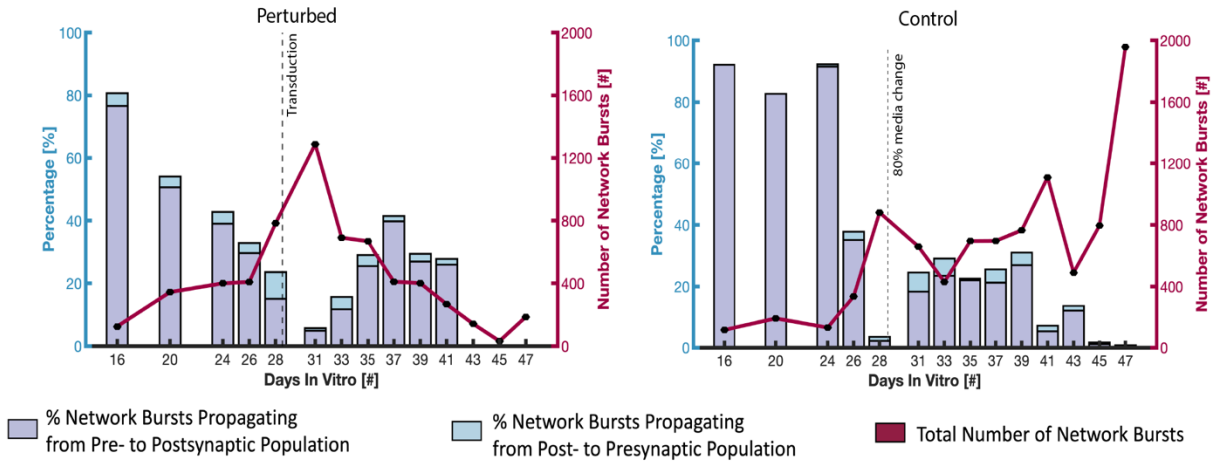

Figure 10. Feedforward burst propagation between pre- and postsynaptic nodes for perturbed (left) and control unperturbed (right) networks. The left y-axis on the graph denotes the percentage of network bursts propagating between the nodes, represented as the bars. The right y-axis denotes the total number of network bursts detected each day represented as the solid line. The x-axis denotes the day in vitro. The stippled line at 28 DIV indicates the day of transduction for the perturbed networks.

We also applied periodical electrical stimulations to the electrode with the highest firing rate in the presynaptic node to assess whether a presynaptic stimulus could evoke a postsynaptic response. The same electrode was stimulated for 1 minute at each recording session between 28 DIV and 47 DIV. We found that electrical stimulation within the presynaptic node of control unperturbed networks produced a spike response followed by a postsynaptic spike response with an average delay time of 20 ms (31 DIV) and 40 ms (35 DIV) **(Figure 11A)**. Control unperturbed networks also produced spike

responses in the presynaptic node at 45 DIV and 47 DIV, although the tuning curves were of lower amplitudes than after previous stimulations. In addition, the spike responses in the postsynaptic node of control unperturbed networks at 45 DIV and 47 DIV were too low to allow for an evaluation of the delay time between the nodes. In contrast, stimulation in the presynaptic node of perturbed networks at 31 and 35 DIV resulted in a presynaptic spike response, with no spike response in the postsynaptic node **(Figure 11B)**. There was no response in presynaptic nor postsynaptic nodes at 45 DIV and 47 DIV in the perturbed networks.

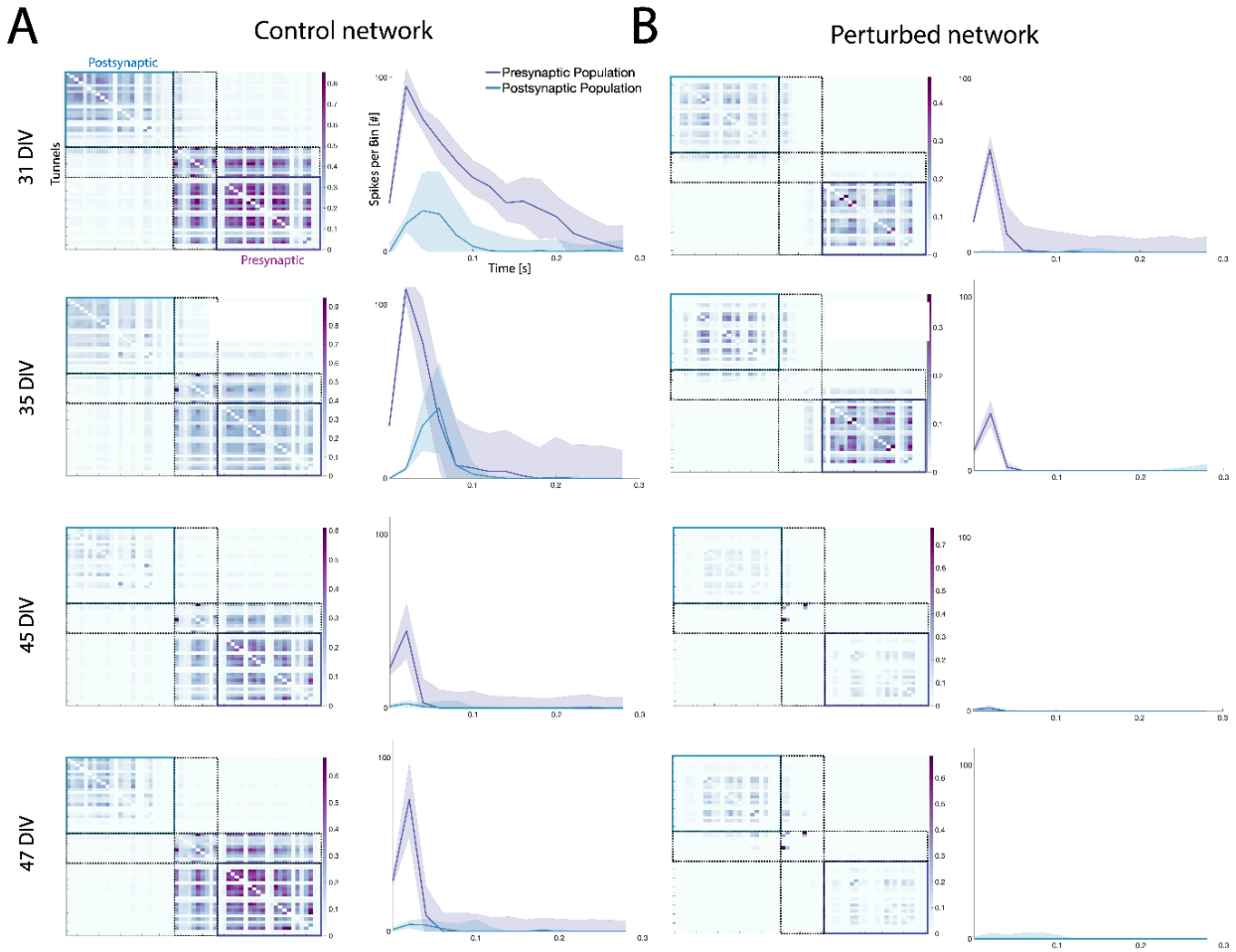

Figure 11. Induced perturbation resulted in progressive decline in presynaptic response to electrical stimulation between the pre-and postsynaptic nodes over time. (A) Mutual information connectivity matrices showing the network activity in chambers and tunnels (left column) and peristimulus time histograms of pre- and postsynaptic responses to electrical stimulations (right column) for control networks at 31, 35, 45 and 47 DIV. (B) Connectivity matrices showing the network activity in chambers and tunnels (left column) and peristimulus time histograms of pre- and postsynaptic responses to electrical stimulations (right column) for perturbed networks at 31, 35, 45 and 47 DIV. The curves show an initial response in the presynaptic network, followed by a delayed response in the postsynaptic network (for control networks) and no postsynaptic response (for perturbed networks). The shaded area denotes the standard error of the mean.

4. Discussion

Engineered neural networks *in vitro* self-organize into complex topologies and produce a complex profile of activity patterns ranging from individual spikes produced by single neurons to high frequency network bursts generated by neural assemblies (Chiappalone et al., 2006; van de Wijdeven et al., 2018; Weir et al., 2023). The development of complex network activity can be attributed to the structural properties of the network, as function tends to co-evolve with structure (Kapucu et al., 2017). Activity typically evolves with the maturity of neurons, and of excitatory and inhibitory synapses. As shown in **Figure 2**, our engineered neural networks expressed both the excitatory neuronal marker CaMKIIa, and the inhibitory neuronal marker GAD65/67 in conjunction with the neuronal marker MAP2 by 21 DIV, strongly indicating the capacity for excitatory – inhibitory synaptic transmission within the maturing networks. This was further verified through recordings of electrophysiological activity, which showed that in healthy conditions, networks developed highly dynamic and complex age-dependent firing activity and network bursts over time, in line with previous studies by us and others (Chiappalone et al., 2006; Chiappalone et al., 2007; Fiskum et al., 2021; van de Wijdeven et al., 2018; Weir et al., 2023).

The structural organization of neural networks is a crucial determining factor for the emergence of complex network dynamics and information processing. In our engineered feedforward networks, we showed that neurites extended from the presynaptic nodes into the microtunnels towards the postsynaptic nodes, thus establishing structural connections. Furthermore, electrical stimulation at 26 DIV confirmed that these networks were functionally interconnected, as evoked activity in the presynaptic node could propagate and elicit a response in the postsynaptic node (illustrated in **Figure 3**), in line with previous findings (Fair et al., 2009; Ma et al., 2018; Winter-Hjelm N, 2023). These results confirm recapitulation of a feedforward network *in vitro*, where information flows in a unidirectional manner, propagating sequentially from input nodes to output nodes (Barzegaran et al., 2022; Markov et al., 2014). Such feedforward hierarchical organizations are found in many parts of the brain (Markov et al., 2014; Siegle et al., 2021), and facilitate fast, efficient information processing between pre- and postsynaptic neuronal assemblies. We also observed spontaneous feedforward burst propagation in control unperturbed networks occurring from 16 DIV to 43 DIV, and perturbed networks from 16 DIV to 41 DIV **(Figure 10).** The ability of the network to spontaneously transmit information between the nodes is an essential factor in determining its functional capacity since this enables the integration of signals that support coordinated, complex information processing (Fauth et al., 2019; Fukushima et al., 2018; Senden et al., 2018). As such, our results confirmed the intended structural and functional organization of engineered feedforward cortical networks, with the presynaptic node providing input to the postsynaptic node **(Figure 3 and Figure 10)**.

465 These engineered feedforward networks also enabled us to selectively induce a perturbation, via AVV
466 mediated expression of human mutated tau in the presynaptic node, and to monitor resulting effects
467 within and between nodes. By utilizing this approach, we can effectively recapitulate and monitor a
468 pathological process at the micro- and mesoscale. Such a process not only induces structural and
469 functional changes in the immediately affected node, but also disrupts both structure and function in
470 the postsynaptic node (Kuhl, 2019; Valderhaug et al., 2021). These findings are highly relevant for
471 advanced modelling of evolving pathological processes in neurodegenerative diseases, such as AD,
472 where an association between the progression of tau pathology and altered transsynaptic activity has
473 been demonstrated [36]. Such transsynaptic spread of tau pathology is attributed to the robust
474 connection loops that exist between the putative origin points of tau pathology in the lateral
475 entorhinal cortex layer II (Braak et al., 1991) and feedforward anatomical sites to hippocampal
476 subregions (Liu et al., 2012; Stepan et al., 2015; Witter, 2007; Witter et al., 2017). This feedforward
477 transsynaptic spread of hyperphosphorylated tau may contribute to structural impairments that
478 disrupt the normal functioning of neural networks. In our study, by quantification of fluorescent
479 signaling of $tau^{202/205}$ and tau^{217} expression, we find prominent differences, i.e., increased tau^{217} in the
480 cytosol of neurons in the perturbed networks compared to the control unperturbed ones, signifying
481 detrimental effects of tau phosphorylation. Normal phosphorylation at $tau^{202/205}$ sites is found in
482 maturing brain and is associated with neural development [40], while tau^{217} phosphorylation is found
483 to be associated with the normal development of postsynaptic sites (Rajbanshi et al., 2023). This
484 means that some phosphorylation of tau at these sites is to be expected in control unperturbed
485 networks as shown in **Figure 6**. Furthermore, studies have shown that the phosphorylation of tau at a
486 single site does not preferentially induce neurotoxic effects (Steinhilb et al., 2007). It appears then
487 that the neurotoxic effects of tau depend on a combined high phosphorylation pattern at multiple
488 sites in axons and/or cytosol, which we have demonstrated in our perturbed networks **(Figure 6)**. In
489 addition, recent findings also reported a correlation between high tau^{217} expression and AD pathology
490 progression (Rajbanshi et al., 2023) associated with synaptic decline. Therefore, our finding of
491 increased expression of both $tau^{202/205}$ and tau^{217} in the cytosol of neurons within the perturbed
492 networks suggests that the introduction of human mutated tau, capable of inducing detrimental
493 synaptic effects, has impacted both the structural and functional dynamics of these networks.

494 This result is further supported by the differences found in the electrophysiological activity of
495 perturbed networks compared to unperturbed controls. Initially, both unperturbed control and
496 perturbed networks had diminished burst propagation between pre- and postsynaptic nodes over
497 time, with very little propagation from 41 DIV in healthy controls, and no propagation after 43 DIV in
498 the perturbed networks, as illustrated in **Figure 10**. The decreased level of spontaneous activity

propagation in healthy networks with age, i.e., DIV, is suggestive of local information processing within nodes, rather than internodal processing. This is further supported by the drastic increase in the total number of bursts detected within nodes of healthy controls (>1800 bursts/recording by 47 DIV), at the same time as the perturbed networks experienced a drastic decline in the total number of bursts within nodes (<10 bursts/recording by 47 DIV) as shown in **Figure 10.** The perturbed networks exhibited differences that can be attributed to increased tau hyperphosphorylation, which, when combined with feedforward propagation between the immediately affected node and the healthy node, precipitated the spread of perturbation effects, leading to disruption in normal synaptic activity across the entire network.

Other studies have found that severity of neuronal loss and atrophy of cortical structures as a result of tau pathology tend to positively correlate with the severity of functional network decline (Adamec et al., 2002; Rascovsky et al., 2005), thus highlighting the complex interrelationship between network structure and function in pathology. The present study revealed such dynamic structural and functional changes in perturbed networks, attributable to the induced expression of human mutated tau at 28 DIV. Between 32 DIV and 52 DIV, we observed progressive neurite retraction from the entry zone near the microtunnels in the presynaptic nodes in the perturbed networks. We also noticed that retraction from the exit zone near the postsynaptic nodes also occurred within weeks of presynaptic retraction as shown in **Figure 7A**. This was not observed in the unperturbed control networks, which maintained a dense neurite network in the zones near the microtunnels in both nodes as seen in **Figure 7B**. The significance of these changes in perturbed networks lies in their potential to adversely affect the network's ability to transmit and integrate information. Prolonged expression of mutant P301L tau exacerbates axonal destabilization (Biswas et al., 2018; Qiang et al., 2018) and impairment of presynaptic terminals (Hunsberger et al., 2021). Furthermore, both maintenance of presynaptic integrity and synaptic plasticity depend on active anterograde and retrograde axonal transport systems (Cai et al., 2011), thus impairment of tau in axons can affect such processes (Lacovich et al., 2017) and severely disrupt synaptic functions between pre- and postsynaptic nodes in perturbed networks. Furthermore, the observed subsequent neurite retraction in the postsynaptic node of the perturbed networks (shown in **Figure 7A)**, suggested that the loss of presynaptic input triggered reorganization within postsynaptic nodes. These observations thus indicated a dynamic process of structural and functional reconfiguration across the entire feedforward network in response to presynaptic node perturbation.

The prominent structural changes observed following induced perturbation occurred concomitantly with changes in the electrophysiological profile of the perturbed networks between 28 DIV and 47 DIV. Prior to perturbation and between 16 DIV and 28 DIV, all networks in our study exhibited similar

533 trends in activity patterns such as firing and burst rate **(Figure 8)**, burst duration and synchrony **(Figure**
534 **9)** and burst propagation **(Figure 10)**. In healthy conditions, gradually increasing firing and burst
535 patterns are crucial for the establishment and maintenance of functional synapses, and the
536 elaboration of the network topology into hierarchical processing. Bursts also contribute to the
537 formation and refinement of neural circuits especially during early network formation (between 9 and
538 21 DIV) [49], where they facilitate the integration of immature neurons into the maturing network. It
539 is therefore expected that all healthy networks would inherently follow this developmental trend of
540 increasing firing and burst rates prior to perturbation. Following the induced expression of human
541 mutated tau, perturbed networks exhibited a steady decline in both firing rate and burst rate in
542 comparison to control unperturbed networks, which continued to display a steady increase over time
543 **(Figure 8)**. Furthermore, these differences in firing rate following perturbation were found to be
544 significant between control unperturbed and perturbed networks in both pre- and postsynaptic
545 nodes. This suggested that perturbed networks became less electrophysiologically active as they
546 underwent structural reorganization, including neurite retraction. The observed decrease in firing and
547 bursting activity also aligned with *in vivo* findings showing that neurons in a mouse model with the
548 Tau-P301 mutation gradually became more hypoactive (Busche et al., 2019). However, Busche et al.,
549 (Busche, 2019) also suggested that the disruption in network activity occurred before any prominent
550 structural tau abnormalities were observed in vivo. We have shown however, that the decline in
551 general network activity correlated strongly with the progressive loss of synaptic connectivity and pre-
552 and postsynaptic neurite reorganization. These changes are highly challenging to detect and correlate
553 *in vivo*.

554 Another interesting result in our study was the significant increase in network burst size and
555 synchrony, as measured by the coherence index, observed in the perturbed networks between 28 DIV
556 and 47 DIV **(Figure 9 E and F)**. Network bursts, which are coordinated patterns of neuronal activity
557 exhibited by multiple interconnected neurons within the network, are ubiquitous for normal network
558 function (Weir et al., 2023). Coordinated neuronal activity also leads to network synchrony (Salinas et
559 al., 2001), and is thus important for information processing, coding, and synaptic integration of
560 distributed signals (Gansel, 2022). Synchrony may also promote activity-dependent establishment of
561 synaptic connections via spike-timing dependent plasticity (STDP) (Anisimova et al., 2022) to support
562 network function. In a recent study by our group, we found that networks that were perturbed by
563 selective silencing of excitatory synaptic transmission also demonstrated increased synchrony during
564 network recovery (Weir et al., 2023). Such behavior may thus be crucial for the network's ability to
565 restore its functional and structural organization within specific time windows after a perturbation.

566 On the other hand, increased synchrony may also have adverse effects, such as facilitating the spread
567 of perturbations through axons and synapses to affect the entire interconnected network (Uhlhaas et
568 al., 2006), as has been found in AD pathology (Liu et al., 2012; Wang et al., 2017). Furthermore,
569 excessive network bursts and synchrony have been implicated in various neurological disorders,
570 including epilepsy, where they signify a disruption in normal network physiology i.e., impaired
571 excitatory-inhibitory dynamics (Kudela et al., 2003; Wu et al., 2015). Therefore, while a degree of
572 network synchrony is necessary for normal functioning, too much can be problematic. This raises a
573 crucial question regarding whether the observed synchrony in the perturbed networks in our study
574 may represent an adaptive or maladaptive network response to induced perturbation.

575 Interestingly, synchrony increased concurrently with neurite retraction at 32 DIV, and while firing and
576 burst rate declined. We found that, following perturbation, networks began exhibiting fewer, yet
577 larger synchronized bursts, which can be interpreted as a homeostatic compensatory response to
578 maintain network activity as the overall firing and burst rates declined. In response to low network
579 activity levels, homeostatic scaling, which occurs gradually and over several hours to days, can
580 increase overall input to counteract hypoactivity (Chowdhury et al., 2018; Turrigiano, 2008). This may
581 explain the observation of increasing synchrony between 31 DIV and 47 DIV **(Figure 9 E and F).**
582 However, increased synchrony could also signify pathophysiological changes in the underlying
583 network since it occurred concomitant with the evolution of induced pathology. *In vivo,* induced
584 perturbation caused by hyperphosphorylated tau can disrupt the structural and functional integrity of
585 the affected network, and subsequently result in increased inflammation leading to apoptotic or
586 necrotic cell death (Dong et al., 2022; Thal et al., 2022). Furthermore, it has been suggested that the
587 presence of diverse connections and pathways within a neural network can provide alternative routes
588 for information flow to reduce the reliance on a single synchronized pathway (Kirst et al., 2016), thus
589 acting as a gatekeeping mechanism to prevent excessive synchrony and enhancing overall network
590 robustness. In our study, as induced perturbation led to progressive structural and functional
591 disruption in the network, it is likely that information flow within the network might have been
592 hindered, as there were insufficient alternative routes to effectively distribute activity, ultimately
593 leading to excessive synchrony. This is further supported by observations in control unperturbed
594 during the same time frame between 31 DIV and 47 DIV. During this time, control networks exhibited
595 significantly higher mean firing and burst rates **(Figure 8)** and comparatively more bursts within nodes
596 **(Figure 10)**, without showing excessive synchrony. These networks also maintained the dense neurite
597 architectures between the nodes. This effectively suggests that the unperturbed control networks
598 possessed the ability to maintain their activity within a dynamic range to prevent excessive network
599 wide activation, an ability which the perturbed networks appeared to gradually lose. Based on these

findings, increased network synchrony after induced perturbation might be associated with the deterioration of overall network function in response to the perturbation, rather than serving as an adaptive purpose.

Lastly, to further investigate whether perturbation affected structural and functional connectivity between the nodes, we applied periodic electrical stimulation to one electrode within the presynaptic node and assessed the postsynaptic response. We found that although control unperturbed exhibited a consistent presynaptic spike response to electrical stimulation, there was a gradual decline in the postsynaptic response over time as illustrated in **Figure 11A**. This could be due to activity dependent long-term synaptic changes in the vicinity of the stimulating electrode, such as a reduction in synapse number or downscaling of synaptic receptors on neurons, as previously reported (Collingridge et al., 2010). Such activity dependent structural changes would likely reduce the amplitude of the presynaptic response, thus reducing the strength of the propagating signal (as shown in **Figure 11A)**. For perturbed networks, we found that there was no response to presynaptic stimulation in the postsynaptic node by 31 DIV (**Figure 11B)**. This outcome was anticipated as we had already observed extensive neurite retraction in the presynaptic node by the specific time point, indicating the severance of connectivity between nodes. No response to stimulation was observed in the presynaptic node at 45 DIV and 47 DIV, which may be due to possible progressive neuron loss in the network, or structural reorganization of any remaining neurons to areas outside the vicinity of the stimulating electrode. Nevertheless, the differences in response to electrical stimulation between perturbed and control unperturbed networks may reflect the functional capacity of each network, although determination of whether these differences were indeed related to the networks´ functional capacity was beyond the scope of this study.

5. Conclusions and future directions

Using engineered two-nodal feedforward neural networks with controllable afferent-efferent connections, we longitudinally monitored and assessed dynamic structural and functional behaviors in healthy conditions and in response to induced perturbation via expression of human mutated tau. We found that prior to perturbation, both control unperturbed and perturbed networks followed a similar developmental trajectory consistent with relevant literature. The effects of the induced perturbation were evident within one week, with perturbed networks exhibiting significant decreases in firing rate, burst rate and total number of bursts in comparison to the relevant increases observed in control unperturbed networks. These changes align with reported adverse effects of tau hyperphosphorylation. Furthermore, over time, while healthy controls showed a steady decline in burst size and synchrony, perturbed networks showed significant increases in both, suggesting that all the activity was contained within a few, large, synchronized network bursts. Increasing synchrony,

634 coupled to neurite retraction and the overall decline in firing and burst rates also suggested that the
635 observed synchrony may be a maladaptive, rather than an adaptive, response. Importantly, the
636 relevant changes seen in the perturbed networks were not observed in healthy controls, suggesting
637 that the changes were attributable to the induced perturbation, rather than physiological endogenous
638 tau expression. Taken together, these findings provide significant new insights into dynamic structural
639 and functional reconfigurations at the micro- and mesoscale in engineered feedforward neural
640 networks as a result of evolving tau-associated pathology.

641 **Data availability statement**

642 The raw data that support the findings of this study will be made available by the authors upon request.

643 **Author Contributions**

644 The author contribution follows the CRediT system. JSW, KSH: Conceptualization, Investigation (Cell
645 experiments; Protocol development and optimization; AAV investigations, Immunocytochemistry and
646 Electrophysiological recordings), Writing – Original Draft, Review and Editing, Illustration. NWH: Methodology,
647 Software, Investigation (chip design & manufacturing, electrophysiology, formal analysis), Writing – Review and
648 Editing. AS, IS: Conceptualization, Methodology, Writing – Review & Editing, Funding acquisition, Supervision.

649 **Funding**

650 This project was funded by The Research Council of Norway (NFR, IKT Pluss; Self-Organizing Computational
651 Substrates (SOCRATES)) Grant number: 27096; NTNU Enabling Technologies and The Liaison Committee for
652 education, research, and innovation in Central Norway.

653 **Acknowledgement**

654 The authors would like to thank Dr. Christiana Bjørkli for the technical support in developing the transduction
655 protocol and gifting us the AAV8-GFP-2a-P301Ltau-virus, originally designed, and produced by Dr. Rajeevkumar
656 Nair Raveendran at the Viral Vector Core Facility, Kavli Institute for Systems Neuroscience. Prof. Michela
657 Chiappalone and Prof. Sergio Martinoia, University of Genova for generously providing the scripts for the Precise
658 Timing Spike Detection algorithm and the logISI burst detection. Prof. Menno P. Witter and Dr. Asgeir Kobro-
659 Flatmoen, Kavli Institute for Systems Neuroscience for kindly reading and proving their feedback. The Research
660 Council of Norway is acknowledged for the support to the Norwegian Micro- and Nano-Fabrication Facility,
661 NorFab, project number 295864.

662 **Conflict of Interest**

663 The authors declare that the research was conducted in the absence of any commercial or financial relationships
664 that could be construed as potential conflict of interest.

References

Adamec, E., Murrell, J. R., Takao, M., Hobbs, W., Nixon, R. A., Ghetti, B., & Vonsattel, J. P. (2002). P301L tauopathy: confocal immunofluorescence study of perinuclear aggregation of the mutated protein. *J Neurol Sci, 200*(1-2), 85-93. doi:10.1016/s0022-510x(02)00150-8

Anisimova, M., van Bommel, B., Wang, R., Mikhaylova, M., Wiegert, J. S., Oertner, T. G., & Gee, C. E. (2022). Spike-timing-dependent plasticity rewards synchrony rather than causality. *Cereb Cortex, 33*(1), 23-34. doi:10.1093/cercor/bhac050

Barzegaran, E., & Plomp, G. (2022). Four concurrent feedforward and feedback networks with different roles in the visual cortical hierarchy. *PLoS Biol, 20*(2), e3001534. doi:10.1371/journal.pbio.3001534

Bauer, U. S., Fiskum, V., Nair, R. R., van de Wijdeven, R., Kentros, C., Sandvig, I., & Sandvig, A. (2022). Validation of Functional Connectivity of Engineered Neuromuscular Junction With Recombinant Monosynaptic Pseudotyped ΔG-Rabies Virus Tracing. *Front Integr Neurosci, 16*, 855071. doi:10.3389/fnint.2022.855071

Biswas, S., & Kalil, K. (2018). The Microtubule-Associated Protein Tau Mediates the Organization of Microtubules and Their Dynamic Exploration of Actin-Rich Lamellipodia and Filopodia of Cortical Growth Cones. *J Neurosci, 38*(2), 291-307. doi:10.1523/jneurosci.2281-17.2017

Brewer, G. J., Boehler, M. D., Ide, A. N., & Wheeler, B. C. (2009). Chronic electrical stimulation of cultured hippocampal networks increases spontaneous spike rates. *J Neurosci Methods, 184*(1), 104-109. doi:10.1016/j.jneumeth.2009.07.031

Bruno, G., Colistra, N., Melle, G., Cerea, A., Hubarevich, A., Deleye, L., . . . Dipalo, M. (2020). Microfluidic Multielectrode Arrays for Spatially Localized Drug Delivery and Electrical Recordings of Primary Neuronal Cultures. *Front Bioeng Biotechnol, 8*, 626. doi:10.3389/fbioe.2020.00626

Braak, H., & Braak, E. (1991). Neuropathological stageing of Alzheimer-related changes. *Acta Neuropathol, 82*(4), 239-259. doi:10.1007/bf00308809

Busche, M. A. (2019). Tau suppresses neuronal activity in vivo, even before tangles form. *Brain, 142*(4), 843-846. doi:10.1093/brain/awz060

Busche, M. A., Wegmann, S., Dujardin, S., Commins, C., Schiantarelli, J., Klickstein, N., . . . Hyman, B. T. (2019). Tau impairs neural circuits, dominating amyloid-β effects, in Alzheimer models in vivo. *Nat Neurosci, 22*(1), 57-64. doi:10.1038/s41593-018-0289-8

Baas, P. W., & Qiang, L. (2019). Tau: It's Not What You Think. *Trends Cell Biol, 29*(6), 452-461. doi:10.1016/j.tcb.2019.02.007

Cai, Q., Davis, M. L., & Sheng, Z. H. (2011). Regulation of axonal mitochondrial transport and its impact on synaptic transmission. *Neurosci Res, 70*(1), 9-15. doi:10.1016/j.neures.2011.02.005

Chiappalone, M., Bove, M., Vato, A., Tedesco, M., & Martinoia, S. (2006). Dissociated cortical networks show spontaneously correlated activity patterns during in vitro development. *Brain Res, 1093*(1), 41-53. doi:10.1016/j.brainres.2006.03.049

Chiappalone, M., Vato, A., Berdondini, L., Koudelka-Hep, M., & Martinoia, S. (2007). Network dynamics and synchronous activity in cultured cortical neurons. *Int J Neural Syst, 17*(2), 87-103. doi:10.1142/s0129065707000968

Chowdhury, D., & Hell, J. W. (2018). Homeostatic synaptic scaling: molecular regulators of synaptic AMPA-type glutamate receptors. *F1000Res, 7*, 234. doi:10.12688/f1000research.13561.1

Collingridge, G. L., Peineau, S., Howland, J. G., & Wang, Y. T. (2010). Long-term depression in the CNS. *Nat Rev Neurosci, 11*(7), 459-473. doi:10.1038/nrn2867

Dong, Y., Yu, H., Li, X., Bian, K., Zheng, Y., Dai, M., . . . Kong, W. (2022). Hyperphosphorylated tau mediates neuronal death by inducing necroptosis and inflammation in Alzheimer's disease. *J Neuroinflammation, 19*(1), 205. doi:10.1186/s12974-022-02567-y

Fair, D. A., Cohen, A. L., Power, J. D., Dosenbach, N. U., Church, J. A., Miezin, F. M., . . . Petersen, S. E. (2009). Functional brain networks develop from a "local to distributed" organization. *PLoS Comput Biol, 5*(5), e1000381. doi:10.1371/journal.pcbi.1000381

Fauth, M. J., & van Rossum, M. C. (2019). Self-organized reactivation maintains and reinforces memories despite synaptic turnover. *Elife, 8*. doi:10.7554/eLife.43717

Fiskum, V., Sandvig, A., & Sandvig, I. (2021). Silencing of Activity During Hypoxia Improves Functional Outcomes in Motor Neuron Networks in vitro. *Front Integr Neurosci, 15*, 792863. doi:10.3389/fnint.2021.792863

Fornito, A., Zalesky, A., & Breakspear, M. (2015). The connectomics of brain disorders. *Nat Rev Neurosci, 16*(3), 159-172. doi:10.1038/nrn3901

Fukuda, T., Heizmann, C. W., & Kosaka, T. (1997). Quantitative analysis of GAD65 and GAD67 immunoreactivities in somata of GABAergic neurons in the mouse hippocampus proper (CA1 and CA3 regions), with special reference to parvalbumin-containing neurons. *Brain Res, 764*(1-2), 237-243. doi:10.1016/s0006-8993(97)00683-5

Fukushima, M., Betzel, R. F., He, Y., van den Heuvel, M. P., Zuo, X. N., & Sporns, O. (2018). Structure-function relationships during segregated and integrated network states of human brain functional connectivity. *Brain Struct Funct, 223*(3), 1091-1106. doi:10.1007/s00429-017-1539-3

Gansel, K. S. (2022). Neural synchrony in cortical networks: mechanisms and implications for neural information processing and coding. *Front Integr Neurosci, 16*, 900715. doi:10.3389/fnint.2022.900715

Gribaudo, S., Tixador, P., Bousset, L., Fenyi, A., Lino, P., Melki, R., . . . Perrier, A. L. (2019). Propagation of α-Synuclein Strains within Human Reconstructed Neuronal Network. *Stem Cell Reports, 12*(2), 230-244. doi:10.1016/j.stemcr.2018.12.007

Götz, J., Halliday, G., & Nisbet, R. M. (2019). Molecular Pathogenesis of the Tauopathies. *Annu Rev Pathol, 14*, 239-261. doi:10.1146/annurev-pathmechdis-012418-012936

Henderson, J. A., & Gong, P. (2018). Functional mechanisms underlie the emergence of a diverse range of plasticity phenomena. *PLoS Comput Biol, 14*(11), e1006590. doi:10.1371/journal.pcbi.1006590

Hunsberger, H. C., Setti, S. E., Rudy, C. C., Weitzner, D. S., Pfitzer, J. C., McDonald, K. L., . . . Reed, M. N. (2021). Differential Effects of Human P301L Tau Expression in Young versus Aged Mice. *Int J Mol Sci, 22*(21). doi:10.3390/ijms222111637

Ide, A. N., Andruska, A., Boehler, M., Wheeler, B. C., & Brewer, G. J. (2010). Chronic network stimulation enhances evoked action potentials. *J Neural Eng, 7*(1), 16008. doi:10.1088/1741-2560/7/1/016008

Ittner, L. M., & Götz, J. (2011). Amyloid-β and tau--a toxic pas de deux in Alzheimer's disease. *Nat Rev Neurosci, 12*(2), 65-72. doi:10.1038/nrn2967

Jackson, J. S., Witton, J., Johnson, J. D., Ahmed, Z., Ward, M., Randall, A. D., . . . Ashby, M. C. (2017). Altered Synapse Stability in the Early Stages of Tauopathy. *Cell Rep, 18*(13), 3063-3068. doi:10.1016/j.celrep.2017.03.013

Kapucu, F. E., Valkki, I., Christophe, F., Tanskanen, J. M. A., Johansson, J., Mikkonen, T., & Hyttinen, J. A. K. (2017). On electrophysiological signal complexity during biological neuronal network development and maturation. *Annu Int Conf IEEE Eng Med Biol Soc, 2017*, 3333-3338. doi:10.1109/embc.2017.8037570

Katsuno, M., Sahashi, K., Iguchi, Y., & Hashizume, A. (2018). Preclinical progression of neurodegenerative diseases. *Nagoya J Med Sci, 80*(3), 289-298. doi:10.18999/nagjms.80.3.289

Kirst, C., Timme, M., & Battaglia, D. (2016). Dynamic information routing in complex networks. *Nat Commun, 7*, 11061. doi:10.1038/ncomms11061

Kopeikina, K. J., Polydoro, M., Tai, H. C., Yaeger, E., Carlson, G. A., Pitstick, R., . . . Spires-Jones, T. L. (2013). Synaptic alterations in the rTg4510 mouse model of tauopathy. *J Comp Neurol, 521*(6), 1334-1353. doi:10.1002/cne.23234

Kudela, P., Franaszczuk, P. J., & Bergey, G. K. (2003). Changing excitation and inhibition in simulated neural networks: effects on induced bursting behavior. *Biol Cybern, 88*(4), 276-285. doi:10.1007/s00422-002-0381-7

Kuhl, E. (2019). Connectomics of neurodegeneration. *Nat Neurosci, 22*(8), 1200-1202. doi:10.1038/s41593-019-0459-3

Lacovich, V., Espindola, S. L., Alloatti, M., Pozo Devoto, V., Cromberg, L. E., Čarná, M. E., . . . Falzone, T. L. (2017). Tau Isoforms Imbalance Impairs the Axonal Transport of the Amyloid Precursor Protein in Human Neurons. *J Neurosci, 37*(1), 58-69. doi:10.1523/jneurosci.2305-16.2016

Liu, L., Drouet, V., Wu, J. W., Witter, M. P., Small, S. A., Clelland, C., & Duff, K. (2012). Trans-synaptic spread of tau pathology in vivo. *PLoS One, 7*(2), e31302. doi:10.1371/journal.pone.0031302

Ma, Z., Ma, Y., & Zhang, N. (2018). Development of brain-wide connectivity architecture in awake rats. *Neuroimage, 176*, 380-389. doi:10.1016/j.neuroimage.2018.05.009

Maccione, A., Gandolfo, M., Massobrio, P., Novellino, A., Martinoia, S., & Chiappalone, M. (2009). A novel algorithm for precise identification of spikes in extracellularly recorded neuronal signals. *J Neurosci Methods, 177*(1), 241-249. doi:10.1016/j.jneumeth.2008.09.026

Markov, N. T., Vezoli, J., Chameau, P., Falchier, A., Quilodran, R., Huissoud, C., . . . Kennedy, H. (2014). Anatomy of hierarchy: feedforward and feedback pathways in macaque visual cortex. *J Comp Neurol, 522*(1), 225-259. doi:10.1002/cne.23458

Menkes-Caspi, N., Yamin, H. G., Kellner, V., Spires-Jones, T. L., Cohen, D., & Stern, E. A. (2015). Pathological tau disrupts ongoing network activity. *Neuron, 85*(5), 959-966. doi:10.1016/j.neuron.2015.01.025

Moore, A. K., Weible, A. P., Balmer, T. S., Trussell, L. O., & Wehr, M. (2018). Rapid Rebalancing of Excitation and Inhibition by Cortical Circuitry. *Neuron, 97*(6), 1341-1355.e1346. doi:10.1016/j.neuron.2018.01.045

Nonaka, T., & Hasegawa, M. (2011). In vitro recapitulation of aberrant protein inclusions in neurodegenerative diseases: New cellular models of neurodegenerative diseases. *Commun Integr Biol, 4*(4), 501-502. doi:10.4161/cib.4.4.15779

Pasquale, V., Martinoia, S., & Chiappalone, M. (2010). A self-adapting approach for the detection of bursts and network bursts in neuronal cultures. *J Comput Neurosci, 29*(1-2), 213-229. doi:10.1007/s10827-009-0175-1

Polanco, J. C., Li, C., Durisic, N., Sullivan, R., & Götz, J. (2018). Exosomes taken up by neurons hijack the endosomal pathway to spread to interconnected neurons. *Acta Neuropathol Commun, 6*(1), 10. doi:10.1186/s40478-018-0514-4

Qiang, L., Sun, X., Austin, T. O., Muralidharan, H., Jean, D. C., Liu, M., . . . Baas, P. W. (2018). Tau Does Not Stabilize Axonal Microtubules but Rather Enables Them to Have Long Labile Domains. *Curr Biol, 28*(13), 2181-2189.e2184. doi:10.1016/j.cub.2018.05.045

Rajbanshi, B., Guruacharya, A., Mandell, J. W., & Bloom, G. S. (2023). Localization, induction, and cellular effects of tau phosphorylated at threonine 217. *Alzheimers Dement*. doi:10.1002/alz.12892

Rascovsky, K., Salmon, D. P., Lipton, A. M., Leverenz, J. B., DeCarli, C., Jagust, W. J., . . . Galasko, D. (2005). Rate of progression differs in frontotemporal dementia and Alzheimer disease. *Neurology, 65*(3), 397-403. doi:10.1212/01.wnl.0000171343.43314.6e

Rubinov, M., Sporns, O., van Leeuwen, C., & Breakspear, M. (2009). Symbiotic relationship between brain structure and dynamics. *BMC Neurosci, 10*, 55. doi:10.1186/1471-2202-10-55

Salinas, E., & Sejnowski, T. J. (2001). Correlated neuronal activity and the flow of neural information. *Nat Rev Neurosci, 2*(8), 539-550. doi:10.1038/35086012

Senden, M., Reuter, N., van den Heuvel, M. P., Goebel, R., Deco, G., & Gilson, M. (2018). Task-related effective connectivity reveals that the cortical rich club gates cortex-wide communication. *Hum Brain Mapp, 39*(3), 1246-1262. doi:10.1002/hbm.23913

Siegle, J. H., Jia, X., Durand, S., Gale, S., Bennett, C., Graddis, N., . . . Koch, C. (2021). Survey of spiking in the mouse visual system reveals functional hierarchy. *Nature, 592*(7852), 86-92. doi:10.1038/s41586-020-03171-x

Steinhilb, M. L., Dias-Santagata, D., Fulga, T. A., Felch, D. L., & Feany, M. B. (2007). Tau phosphorylation sites work in concert to promote neurotoxicity in vivo. *Mol Biol Cell, 18*(12), 5060-5068. doi:10.1091/mbc.e07-04-0327

Stepan, J., Dine, J., & Eder, M. (2015). Functional optical probing of the hippocampal trisynaptic circuit in vitro: network dynamics, filter properties, and polysynaptic induction of CA1 LTP. *Front Neurosci, 9*, 160. doi:10.3389/fnins.2015.00160

Takao, K., Okamoto, K., Nakagawa, T., Neve, R. L., Nagai, T., Miyawaki, A., . . . Hayashi, Y. (2005). Visualization of synaptic Ca2+ /calmodulin-dependent protein kinase II activity in living neurons. *J Neurosci, 25*(12), 3107-3112. doi:10.1523/jneurosci.0085-05.2005

Tarawneh, R., & Holtzman, D. M. (2012). The clinical problem of symptomatic Alzheimer disease and mild cognitive impairment. *Cold Spring Harb Perspect Med, 2*(5), a006148. doi:10.1101/cshperspect.a006148

Thal, D. R., & Tomé, S. O. (2022). The central role of tau in Alzheimer's disease: From neurofibrillary tangle maturation to the induction of cell death. *Brain Res Bull, 190*, 204-217. doi:10.1016/j.brainresbull.2022.10.006

Timme, N. M., & Lapish, C. (2018). A Tutorial for Information Theory in Neuroscience. *eNeuro, 5*(3). doi:10.1523/eneuro.0052-18.2018

Turrigiano, G. G. (2008). The self-tuning neuron: synaptic scaling of excitatory synapses. *Cell, 135*(3), 422-435. doi:10.1016/j.cell.2008.10.008

Uhlhaas, P. J., & Singer, W. (2006). Neural synchrony in brain disorders: relevance for cognitive dysfunctions and pathophysiology. *Neuron, 52*(1), 155-168. doi:10.1016/j.neuron.2006.09.020

Valderhaug, V. D., Heiney, K., Ramstad, O. H., Bråthen, G., Kuan, W. L., Nichele, S., . . . Sandvig, I. (2021). Early functional changes associated with alpha-synuclein proteinopathy in engineered human neural networks. *Am J Physiol Cell Physiol, 320*(6), C1141-c1152. doi:10.1152/ajpcell.00413.2020

Vale, C., Alonso, E., Rubiolo, J. A., Vieytes, M. R., LaFerla, F. M., Giménez-Llort, L., & Botana, L. M. (2010). Profile for amyloid-beta and tau expression in primary cortical cultures from 3xTg-AD mice. *Cell Mol Neurobiol, 30*(4), 577-590. doi:10.1007/s10571-009-9482-3

van de Wijdeven, R., Ramstad, O. H., Bauer, U. S., Halaas, Ø., Sandvig, A., & Sandvig, I. (2018). Structuring a multi-nodal neural network in vitro within a novel design microfluidic chip. *Biomed Microdevices, 20*(1), 9. doi:10.1007/s10544-017-0254-4

van de Wijdeven, R., Ramstad, O. H., Valderhaug, V. D., Köllensperger, P., Sandvig, A., Sandvig, I., & Halaas, Ø. (2019). A novel lab-on-chip platform enabling axotomy and neuromodulation in a multi-nodal network. *Biosens Bioelectron, 140*, 111329. doi:10.1016/j.bios.2019.111329

Wagenaar, D. A., Pine, J., & Potter, S. M. (2006). An extremely rich repertoire of bursting patterns during the development of cortical cultures. *BMC Neurosci, 7*, 11. doi:10.1186/1471-2202-7-11

Wagenaar, D. A., & Potter, S. M. (2002). Real-time multi-channel stimulus artifact suppression by local curve fitting. *J Neurosci Methods, 120*(2), 113-120. doi:10.1016/s0165-0270(02)00149-8

Wang, Y., Balaji, V., Kaniyappan, S., Krüger, L., Irsen, S., Tepper, K., . . . Mandelkow, E. M. (2017). The release and trans-synaptic transmission of Tau via exosomes. *Mol Neurodegener, 12*(1), 5. doi:10.1186/s13024-016-0143-y

Weir, J. S., Christiansen, N., Sandvig, A., & Sandvig, I. (2023). Selective inhibition of excitatory synaptic transmission alters the emergent bursting dynamics of in vitro neural networks. *Front Neural Circuits, 17*, 1020487. doi:10.3389/fncir.2023.1020487

Winter-Hjelm N, T. Å. B., Sikoriski P, Sandvig A, Sandvig I. (2023). Structure-Function Dynamics of Engineered, Modular Neuronal Networks with Controllable Afferent-Efferent Connectivity. *Journal of Neural Engineering* doi:DOI 10.1088/1741-2552/ace37f

Witter, M. P. (2007). The perforant path: projections from the entorhinal cortex to the dentate gyrus. *Prog Brain Res, 163*, 43-61. doi:10.1016/s0079-6123(07)63003-9

Witter, M. P., Doan, T. P., Jacobsen, B., Nilssen, E. S., & Ohara, S. (2017). Architecture of the Entorhinal Cortex A Review of Entorhinal Anatomy in Rodents with Some Comparative Notes. *Front Syst Neurosci, 11*, 46. doi:10.3389/fnsys.2017.00046

Wu, Y., Liu, D., & Song, Z. (2015). Neuronal networks and energy bursts in epilepsy. *Neuroscience, 287*, 175-186. doi:10.1016/j.neuroscience.2014.06.046

Yamamoto, H., Moriya, S., Ide, K., Hayakawa, T., Akima, H., Sato, S., . . . Hirano-Iwata, A. (2018). Impact of modular organization on dynamical richness in cortical networks. *Sci Adv, 4*(11), eaau4914. doi:10.1126/sciadv.aau4914